

# SANDIA REPORT

SAND99-1483

Unlimited Release

Printed June 1999

## Performance and Design Analysis of a 250-kW, Grid-Connected Battery Energy Storage System

Benjamin L. Norris and Greg J. Ball

Prepared by  
Sandia National Laboratories  
Albuquerque, New Mexico 87185 and Livermore, California 94550

Sandia is a multiprogram laboratory operated by Sandia Corporation,  
a Lockheed Martin Company, for the United States Department of  
Energy under Contract DE-AC04-94AL85000.

Approved for public release; further dissemination unlimited.



**Sandia National Laboratories**

Issued by Sandia National Laboratories, operated for the United States Department of Energy by Sandia Corporation.

**NOTICE:** This report was prepared as an account of work sponsored by an agency of the United States Government. Neither the United States Government, nor any agency thereof, nor any of their employees, nor any of their contractors, subcontractors, or their employees, make any warranty, express or implied, or assume any legal liability or responsibility for the accuracy, completeness, or usefulness of any information, apparatus, product, or process disclosed, or represent that its use would not infringe privately owned rights. Reference herein to any specific commercial product, process, or service by trade name, trademark, manufacturer, or otherwise, does not necessarily constitute or imply its endorsement, recommendation, or favoring by the United States Government, any agency thereof, or any of their contractors or subcontractors. The views and opinions expressed herein do not necessarily state or reflect those of the United States Government, any agency thereof, or any of their contractors.

Printed in the United States of America. This report has been reproduced directly from the best available copy.

Available to DOE and DOE contractors from  
Office of Scientific and Technical Information  
P.O. Box 62  
Oak Ridge, TN 37831

Prices available from (703) 605-6000  
Web site: <http://www.ntis.gov/ordering.htm>

Available to the public from  
National Technical Information Service  
U.S. Department of Commerce  
5285 Port Royal Rd  
Springfield, VA 22161

NTIS price codes  
Printed copy: A05  
Microfiche copy: A01



SAND99-1483  
Unlimited Release  
Printed June 1999

# **Performance and Design Analysis of a 250-kW, Grid-Connected Battery Energy Storage System**

Benjamin L. Norris  
Gridwise Engineering Company  
121 Starlight Place  
Danville, California 94526

Greg J. Ball  
Energy and Environmental Economics, Inc.  
353 Sacramento St., Suite 1540  
San Francisco, CA 94111

## **Abstract**

This report documents the assessment of performance and design of a 250-kW prototype battery energy storage system developed by Omnion Power Engineering Company and tested by Pacific Gas and Electric Company, both in collaboration with Sandia National Laboratories. The assessment included system performance, operator interface, and reliability. The report also discusses how to detect failed battery strings with strategically located voltage measurements.

## **Acknowledgments**

The authors would like to thank the Energy Storage Systems Program at Sandia National Laboratories and the Department of Energy's Office of Power Technologies for sponsoring this work. Sandia is a multiprogram laboratory operated by Sandia Corporation, a Lockheed Martin Company, for the United States Department of Energy under Contract DE-AC04-94AL85000. The work described in this report was performed for Sandia National Laboratories under Contract AX-6291.

## Contents

Acknowledgments .....	ii
Acronyms .....	v
Executive Summary .....	ES-1
<b>1. Background.....</b>	<b>1-1</b>
<b>2. System Design Issues .....</b>	<b>2-1</b>
Battery System.....	2-1
Battery Technology .....	2-1
Charge Control .....	2-1
Electrical Interface .....	2-1
DC Interface .....	2-1
Utility Interface Requirements.....	2-1
Power Factor Control.....	2-2
Harmonics.....	2-2
Audio Noise.....	2-3
Radio Frequency Interference.....	2-3
Islanding .....	2-3
Communications and Control .....	2-3
Load-Following Dispatch Strategy .....	2-3
SCADA Implementation.....	2-4
<b>3. Thermal Regulation .....</b>	<b>3-1</b>
Data Acquisition.....	3-1
Temperature Distributions.....	3-1
Air Flow Design .....	3-6
Temperature Impacts on String Voltages .....	3-6
Temperature Impacts on Capacity.....	3-9
<b>4. End-of-Life Prediction .....</b>	<b>4-1</b>
String Failure.....	4-1
Goal of Analysis .....	4-1
Voltage Imbalance.....	4-1
Discovery of Failed Batteries .....	4-1
Imbalance Voltage Measurement.....	4-2
Imbalance Voltage Characteristics .....	4-2
Quarter-String Measurements.....	4-5
Additional Considerations .....	4-6
<b>5. Conclusions .....</b>	<b>5-1</b>
Battery Technology .....	5-1
Charge Control .....	5-1
Utility Protection .....	5-1
Load Following .....	5-1
Thermal Regulation.....	5-1
End-of-Life Prediction.....	5-1
<b>6. References .....</b>	<b>6-1</b>
Appendix A – Data Acquisition .....	A-1
Appendix B – Points List .....	B-1
Appendix C – List of Tests .....	C-1

## Figures

ES-1. BESS communications scheme over utility SCADA network.....	ES-1
ES-2. Correlation between discharge temperatures and cell capacity. ....	ES-2
ES-3. Sample quarter-string voltages showing failure in segment Q2.....	ES-3
2-1. Distribution line loading with (a) no battery storage, (b) “block” discharge of 100 kW, and (c) load following dispatch with 100-kW peak.....	2-4
2-2. Control over existing utility SCADA communications network.....	2-5
3-1. Module and container layouts.....	3-2
3-2. String voltages for Modules 1 and 8 during 40-minute discharges on (a) November 17, 1993, and (b) February 21, 1994. ....	3-3
3-3. Battery temperatures during 40-minute discharges on (a) November 17, 1993, before air flow modifications, and (b) February 24, 1994, after air flow modifications. ....	3-4
3-4. Average battery temperatures on (a) November 17, 1993, and (b) February 21, 1994. ....	3-5
3-5. Forced air circulation scheme in PM250 prototype container, after modifications. ....	3-6
3-6. Air circulation within the modules. ....	3-6
3-7. End-of-discharge voltages on November 17, 1993, for all 48 batteries in (a) Module 1 and (b) Module 8.....	3-7
3-8. Relationship between EOD voltage and average discharge temperature for (a) Module 1 and (b) Module 8.....	3-8
3-9. Distribution of Module 1 EOD voltages by tray level.....	3-10
3-10. Distribution of Module 8 EOD voltages by tray level.....	3-11
3-11. String imbalance for Modules 1 and 8 during 40-minute discharge.....	3-12
3-12. Cell capacity versus average discharge temperature.....	3-12
4-1. Module 1 average battery voltage and failed battery voltage during early qualifying tests.....	4-2
4-2. Eight string imbalance voltages.....	4-3
4-3. Voltage imbalance measurement circuit.....	4-3
4-4. Module 1 imbalance voltages over the course of several baseline tests.....	4-4
4-5. Module 1 average, battery #9 and #43 voltages during Baseline test #6.....	4-4
4-6. Imbalance voltage histories for (a) Module 2 and (b) Module 3.....	4-5
4-7. Module 1, Baseline 1; Average battery voltage in each quarter string relative to string average.....	4-7
4-8. Module 1, Baseline 6; Average battery voltage in each quarter string relative to string average.....	4-7

## Tables

1-1. Container and Module Specifications.....	1-1
2-1. IEEE 519 (1991) Current Harmonic Limits for Distributed Generation.....	2-2
3-1. Battery Temperatures During 40-minute Discharge Tests.....	3-2
3-2. Regression Statistics Showing Correlation Between Average Discharge Temperature and EOD Voltage.....	3-9

## **Acronyms**

BESS	battery energy storage system
CFM	cubic feet per minute
DAS	data acquisition system
EOD	end of discharge
EOL	end of life
HVAC	heating, ventilation, and air conditioning
IEEE	Institute of Electrical and Electronics Engineers
IGBT	integrated gate bipolar transistor
PCS	power conversion system
PG&E	Pacific Gas and Electric Company
RFI	radio frequency interference
RTU	remote terminal unit
SCADA	supervisory control and data acquisition
SOC	state of charge
THD	total harmonic distortion

This page intentionally left blank.

## Executive Summary

A prototype 250-kW battery energy storage system was developed by Omnion Power Engineering Co. from 1991 through 1993 and tested in 1993 and 1994 by Pacific Gas and Electric Company. Both companies worked in collaboration with Sandia National Laboratories. The testing project provides a foundation for assessing system-level design issues related to grid-connected energy storage technologies.

A number of design issues are explored based upon the experience with the prototype unit's system performance, operator interface, and reliability. In addition, a methodology is developed for detecting failed battery strings through the use of strategically located voltage measurements.

### System Design Issues

System design issues include the following:

- **Battery technology.** The test performance suggests that the lead-acid battery technology selected for demonstration in the prototype PM250, while produced in high volumes to ensure quality control and low initial cost, may not meet the cycling requirements of utility peak shaving applications. Other battery technologies promise enhanced life and higher energy density.

Advanced charging methodologies, made possible through enhanced voltage and current control

of integrated gate bipolar transistor power conversion equipment, promise to extend battery service life and provide greater reliability.

- **Utility Interconnection.** Battery energy storage system (BESS) designers must meet various protection requirements before connecting the system to the grid. Independent power producers and cogenerators generally meet these requirements through standard mechanical relays. Battery energy storage systems, however, may eliminate the cost of such relays by using the inherent detection and disconnect capabilities of modern solid-state power conversion equipment. Utility acceptance of this approach is increasing.
- **Dispatch Strategies.** Load-following dispatch provides peak load reduction with minimal battery hardware investment. However, the communications schemes required to implement load following in a utility environment are complex, as illustrated in Figure ES-1, and implementation requires some customization for compatibility with existing supervisory control and data acquisition (SCADA) infrastructure. The control interface is designed to simplify information presented to dispatch operators, and most of the control intelligence resides at the remote BESS.

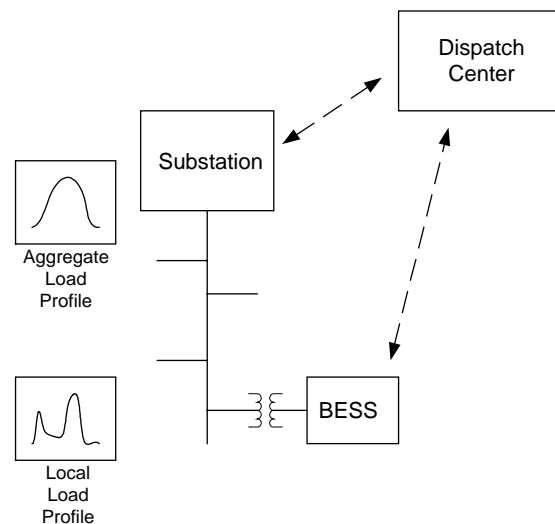


Figure ES-1. BESS communications scheme over utility SCADA network.

*Thermal Regulation*

During testing, thermal gradients within the battery strings were identified as a potential cause of premature string failure. In response, the manufacturer modified the airflow design in order to reduce the temperature variability among batteries. A high-capacity blower was added to the thermal regulation system, and baffling was introduced to direct air currents across batteries for enhanced, uniform cooling. As a result, thermal gradients within and between modules were significantly reduced.

Variations among battery temperatures are shown to correlate strongly with variability in end-of-discharge voltages. Strings with poor thermal regulation show a wide range of variability in voltage distributions in comparison to strings under more controlled thermal conditions.

In addition to voltage distributions, end-of-discharge voltage levels are shown to be strongly correlated with temperature. String segments that were at higher temperatures displayed higher end-of-discharge voltages, which contributed to overall string imbalance. Cell capacities were calculated by integrating the energy discharged over a high-rate test, and these were correlated with average battery discharge temperatures as shown in Figure ES-2.

*End-of-life Prediction*

Measuring voltage across a mid-string grounded resistor (a measure of voltage imbalance) during testing proved to be a low-cost and simple means to characterize the health of the string. If such a methodology could be validated, it would eliminate the need to monitor individual battery voltages in the string.

This investigation shows that while string imbalance is an indicator of cell failure, it is inadequate to detect failure when the effects of two shorted cells counterbalance each other on opposite sides of the string.

The analysis therefore suggests an improved technique that uses quarter-string measurements, in which battery voltages in four separate string segments are compared to the string average. This technique is shown to overcome the counterbalance problem and provide greater accuracy with two additional voltage tap points. Figure ES-3 illustrates how the quarter-string technique detected a failure in a string segment.

The technique can be used to schedule battery replacements and eliminate unnecessary downtime. If used on systems in the field, it would lower the life-cycle cost of the BESS by maximizing battery string life and providing coordinated replacements.

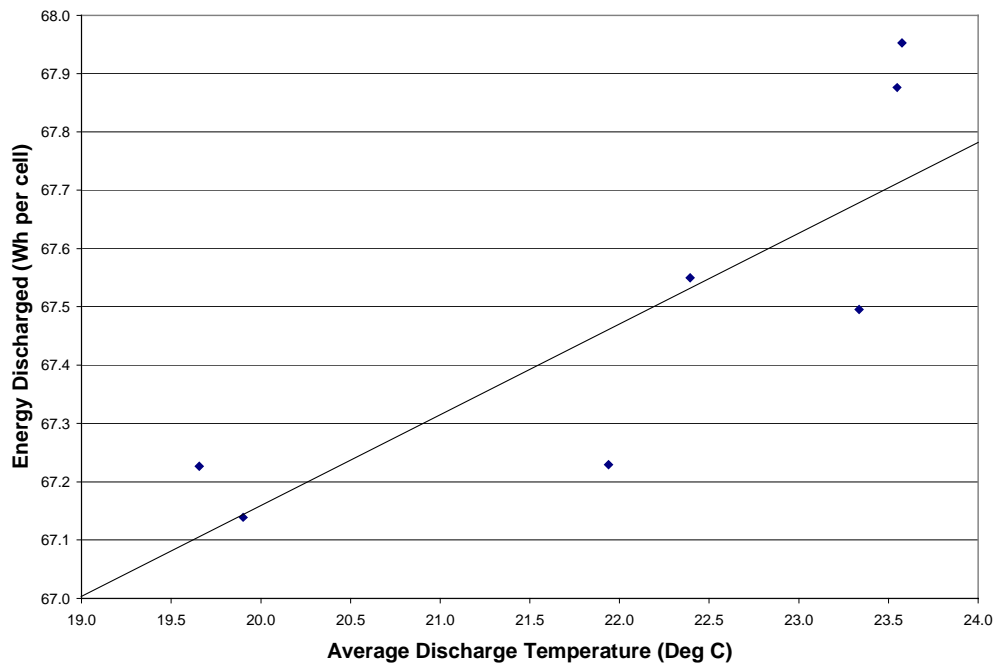


**Figure ES-2. Correlation between discharge temperature and cell capacity.**

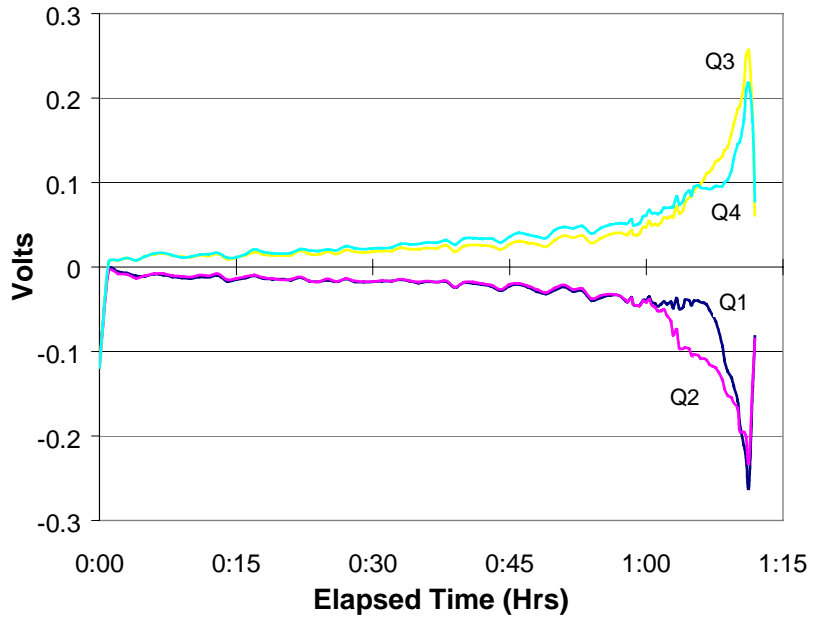


Figure ES-3. Sample quarter-string voltages compared to string average showing failure in segment Q2.

This page intentionally left blank.

# 1. Background

In October 1993 an advanced 250-kW grid-connected battery energy storage system (BESS) was delivered to Pacific Gas and Electric Company (PG&E) for testing at their Modular Generation Test Facility in San Ramon, California, in collaboration with Sandia National Laboratories.

The prototype BESS, under the trade name *PM250*, was designed for utility “peak shaving” applications to provide strategic load management capability on overburdened electric distribution circuits. The system could be placed on the load side of distribution transformers and programmed to discharge energy during peak load periods, thereby relieving line and transformer loading and keeping oil and winding temperatures in check. Battery charging was to be performed off-peak to minimize cost of energy and avoid local capacity constraints.

The system was developed by Omnion Power Engineering Company with support from the U.S. Department of Energy and Sandia National Laboratories beginning in 1991. The design and operation of the system is discussed in detail in SAND97-1276 (Corey, 1998). A customized shipping container housed eight battery/power conditioning modules, paralleled on an AC bus. The overall design specifications are shown in Table 1-1.

Before placing the unit in the field under distribution operators control, PG&E decided to subject the unit to a series of tests under controlled conditions (Ball, 1995). These tests were designed to

- gain utility experience with installation and operation
- test safety systems, such as shutdown in the event of fire or excessive hydrogen concentration
- demonstrate system controls, including compatibility with PG&E communications standards
- verify utility interface protective functions and the quality of power injected into the utility grid
- measure key performance parameters, such as round-trip energy efficiency and storage capacity under different rates of discharge
- demonstrate various operating modes, such as block loading, opportunity charging, and load following (requiring system response to utility-supplied real-time load information)
- characterize the system with respect to audio noise and radio frequency interference (RFI) emissions

The purpose of the present analysis is to investigate various performance and design issues of BESSs, drawing primarily upon data collected during the course of *PM250* testing at PG&E.

The analysis focuses heavily upon issues related to thermal management of battery strings and methods for predicting battery end of life (EOL). Thermal gradients within the strings were identified early in the testing as a potential cause of premature failure, and the preliminary investigation prompted the manufacturer to modify the air flow design in order to reduce the variability among batteries. This investigation extends that work by addressing the thermal impacts on voltage distributions and cell capacities.

The PG&E testing also revealed that voltage imbalance between the positive and negative sections of the string may be a good predictor of EOL. Voltage measurements taken across a mid-string grounded resistor (a measure of voltage imbalance) provided a low cost and simple means to characterize the health of the string. If the technique could be validated, it would eliminate the need to monitor individual battery voltages in the string.

**Table 1-1. Container and Module Specifications**

	Container	Module
Utility Interface	480 Vac; 3-phase	252 Vac; 3-phase
Capacity	250 kW/150 kWh	31.25 kW/18.75 kWh
Configuration	8 modules, central control system and HVAC	48 series-connected batteries, power converter and control
Current THD	Less than 5%	N/A
Power Factor	Unity/Controllable	Unity/Controllable
Dimensions	15'L × 7.8'W × 10.8'H	4.8'L × 3.3'W × 4.3'H
Weight	38,000 lb	4000 lb (est)

*BACKGROUND*

This analysis continues the earlier work, with the goal of validating the string imbalance measurement. Issues were explored related to string imbalance as a predictor of EOL, and develops the alternative technique of quarter-string measurements.

In addition to the analysis of string issues, this report explores system-level design issues determined to be important during the PG&E testing. Battery selection, the grid interface, and communications and control must all be addressed by BESS designers for the technology to be successful.

## 2. System Design Issues

### Battery System

#### Battery Technology

Lead-acid batteries remain the dominant choice for grid-connected energy storage systems. While advanced battery technologies promise enhanced energy storage densities, greater cycling capabilities, higher reliability, and lower cost, they have not yet reached production levels necessary to meet market cost and quality control requirements.

The PM250 employed a high-production volume flooded battery in order to take advantage of quality control and low cost. The life-cycle testing was generally disappointing because of early battery failures, although it is unclear whether rigorous factory testing or extended periods of downtime at low charge states were responsible.

Whether or not the battery selected for demonstration in the PM250 prototype can achieve cycle lives commensurate with the demands of utility peak shaving applications, energy density constraints may limit market penetration to small niche applications. For wide-scale deployment in utility and industrial power management applications, it is clear that significantly higher storage densities will be required. Recent advancements in valve-regulated lead-acid battery designs and enhanced understanding of operating constraints may provide incremental improvement of BESS life-cycle costs.

Advanced electrochemical couples such as zinc-bromine may provide substantial energy-density and cost improvements, but these have yet to reach a significant commercial status (Virmani, 1994).

#### Charge Control

The application of an appropriate and effective charge controller is one of the most important aspects of a good battery system design. Most of the battery-related problems that occur in energy applications, such as hybrid systems, are related to the under- or over-charging of battery strings. At best, a poor charger will cause a lower than expected cycle life by not providing adequate recharge. At worst, a badly designed charger can cause catastrophic battery failures if voltage limits are exceeded.

The PM250 incorporated a proprietary autocharge regimen that was expected to increase reliability and life. With advances in integrated gate bipolar transistor (IGBT) power conditioning equipment, battery charging is no longer limited to constant current and constant voltage regimes. Instead, charging can include any time functions of current and voltage. This appears to be a promising area of design optimization.

### Electrical Interface

#### DC Interface

The design of a DC interface involves balancing the advantages of high DC voltages for improved DC/AC inverter efficiency and performance with the cost and size penalties of the DC protection equipment. High-voltage DC breakers and switches (for example, 600 Vdc or more) can be far more expensive than their AC counterparts. National Electric Code requirements for DC voltages at these high levels are more rigorous as well.

On the other hand, power conversion systems (PCSs) (or inverters) are most efficient at the higher voltages that allow them to generate utility-compatible AC without the addition of a boost stage. The higher voltages also significantly reduce the wire and cable size needed to interconnect the battery to the transformer and utility.

The design approach of the PM250 is to avoid high-cost DC approach by standardizing on a module-level AC interface. This approach provides for enhanced safety because the customer is denied access to the internal module and is consequently never exposed to DC voltages. The AC module interface is also familiar to utility and facility electrical personnel.

#### Utility Interface Requirements

Depending on the size and application of a system, the utility protection requirements can be a costly component of the total system cost. Typical protection requirements include relays and meters that detect ground faults, under- and over-voltage and frequency conditions, AC over-current, DC injection (DC biasing of the AC interconnect transformer),

extreme DC bus voltages, loss of synchronization, blown fuses, and control communication errors.

Interface standards have been developed by utilities over recent years largely in response to the Public Utility Regulatory Policies Act—mandated power transactions. Requirements are well defined for rotating generators found at independent power producers and cogenerators; however, protection schemes that incorporate solid-state inverters and power conditioning equipment are not well established.

Protection schemes for large-scale power producers are generally accomplished with standard mechanical relays. However, modern inverter technologies can provide most of these protection features inherently, and their use in lieu of mechanical relays is gradually gaining acceptance in the utility industry [Institute of Electrical and Electronics Engineers (IEEE) Power System Relaying Committee, 1994]. This trend will help reduce balance of system costs by eliminating the cost of relays.

Some photovoltaic inverters have been pre-approved by utilities, greatly simplifying the installation process. Pre-approvals lower the overall installation cost because utility protection engineers will be familiar with the equipment and will not have to review each installation on a case-by-case basis. Therefore, BESS manufacturers will benefit from standardizing products and obtaining pre-approvals where possible.

## Power Factor Control

Nearly all modern power converter technologies are designed for four-quadrant operation and can provide power factor control in either charge or discharge mode. The benefit of this control is that the system does not appear to the utility as an unwanted consumer of reactive power, and in fact can dynamically produce reactive power to improve voltage regulation for the utility.

## Harmonics

Power converters (and other sources and loads) may be required to meet limits defined in the IEEE 519 standard for generator and load harmonics (IEEE, 1991). These limits are defined in terms of the odd harmonic multiples (3, 5, 7, etc.) of the fundamental frequency (60 Hz). The IEEE 519 standard limits the individual harmonics (as a percentage of the fundamental) as well as the root-square sum of the combined harmonics, known as total harmonic distortion (THD). The THD limits as they are specifically defined for generation systems on distribution circuits are listed in Table 2-1 below.

In the past, the concern and subsequently the measurement of harmonic components from generation sources have been limited to the first 50 harmonics, or up to 3 kHz. This is because in standard rotating machinery, the harmonic level at higher frequencies is virtually non-existent, and older (thyristor-based) converters have negligible high-frequency harmonics. In advanced power converters, however, this is not the case. Switching frequencies greater than 3 kHz are now common.

For example, the PM250 module converters each switch at about 3 kHz. However, their combined waveforms are synchronized with appropriate phase delays to reduce the total ripple on the output current. The resultant system currents contain harmonics in multiples of 3 kHz up to 24 kHz, which are then further attenuated by filter capacitors. The average of several THD measurements taken at the 480 Vac output of the container was 3.3%, well within the 5% limit set forth in the IEEE 519 and PG&E specifications (Ball, 1995). The proportion of the 3-kHz component to the 250-kVA 60-Hz component measured less than the specific IEEE 519 limit of 0.3% for frequencies above 2.1 kHz.

**Table 2-1. IEEE 519 (1991) Current Harmonic Limits for Distributed Generation**

Harmonic Order	< 11th	11th-17th	17th-23rd	23rd-35th	>35th	THD
Magnitude relative to the 60 Hz component	4.0%	2.0%	1.5%	0.6%	0.3%	5%

## Audio Noise

Audio noise can be significant in large converters that use today's technologies. Small inverters make use of devices that can switch at frequencies beyond the audible range, but larger inverters such as the PM250 switch in the 3 to 10 kHz range. Currents oscillating at these frequencies will induce vibrations in filter inductors and may be amplified by metallic mountings to the system enclosure.

This was the case with the PM250, which produced noise averaging 71 dBA, measured one foot from the container at full kVA output—roughly equivalent to the noise produced by a 20-MVA substation transformer. Noises at this level may be an issue depending on the siting of a system. California city and county ordinances, for example, typically require equipment not to exceed 40 dBA at a customer property line. For the prototype build of the PM250 to meet this requirement, it would need to be placed roughly 300 feet from the property line of a residence or other customer.

Subsequent builds of the container have employed measures to reduce noise, and these are expected to overcome noise problems for most sites. These measures include applying noise-attenuating material to the interior surfaces of the container. Another method (Ball, 1995) would be to isolate the sources of vibration from the container, for example, providing vibration isolation pads for inverter inductors and transformers.

## Radio Frequency Interference

Radio frequency interference (RFI) can be an important issue with advanced inverter technologies, because of their use of high frequency switching methods. Measurement techniques and compliance guidelines are set forth by the Federal Communications Commission Code of Federal Regulations. Utility or industrial plant applications may be exempt from some of these regulations, but they still must comply to sections dealing with harmful interference.

## Islanding

Islanding refers to the condition that exists when a generating source continues to supply power to local

loads unintentionally after an up-line breaker or other disconnecting device has operated. For this to occur, the remaining load isolated down-line from the point of disconnect (the "island") must be roughly equivalent to the generator output, such that the transfer does not sufficiently jolt the system voltage or frequency relays. Islanding is desirable in some cases for backup generation purposes, but when unexpected, it creates a potential hazard to utility maintenance personnel (and possibly the general public) who assume the circuit is dead.

Another concern surrounding islanding is the scenario of the utility reclosing on the island when the two separate supply voltages are out of phase, possibly resulting in damaging current surges to sensitive loads.

A common islanding prevention method, such as that used in the PM250, is one in which the inverter continually attempts to drive the frequency below 60 Hz. When the utility is present, the frequency is reset every cycle by a phase-locked loop. If the utility is not present, however, the frequency is forced downward until the system is tripped off by the under-frequency relay. This method may fail in cases where inertia from reactive or rotating loads maintains the frequency, but even in such cases, the system usually becomes unstable within a few seconds and shuts down.

## Communications and Control

### Load-Following Dispatch Strategy

As the capital cost of a BESS increases with kWh storage capacity, it is of interest to explore "smart" dispatch strategies, such as load-following, which are able to provide enhanced kW load relief in comparison to constant output "block" loading.

Figure 2-1 illustrates the potential benefit of employing a load-following dispatch strategy with a BESS. Figure 2-1(a) shows a hypothetical daily load profile on a distribution line. The peak of this load can be "shaved" by discharging the BESS at the peak load time, triggered by either a clock or an indicator of load threshold, illustrated as a 100-kW constant output ("block") discharge in Figure 2-1(b). Provided that the battery output is timed properly, the 100-kW output of the battery will result in a 100-kW peak load reduction on the line.

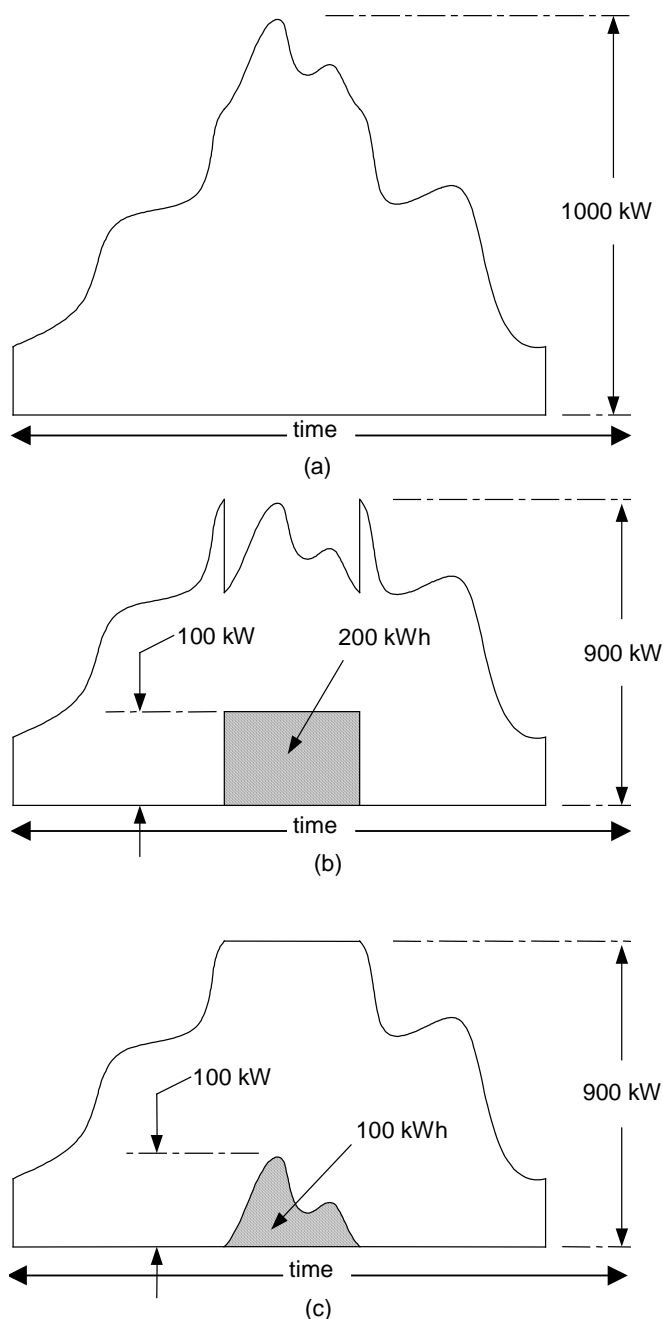


**Figure 2-1. Distribution line loading with (a) no battery storage, (b) “block” discharge of 100 kW, and (c) load following dispatch with 100-kW peak.**

An equivalent amount of load reduction, however, can be achieved with a smaller battery energy capacity through the use of a smart dispatch strategy, illustrated in Figure 2-1(c) as a 100-kW (peak) load-following dispatch. This strategy involves varying the output of the battery in response to instantaneous fluctuations in load. In this example, the load-following strategy achieves the same 100-kW peak

load reduction while consuming only half the energy of the block load.

### SCADA Implementation

This potential load-following benefit was the motivating force behind the design of the PM250 prototype supervisory control and data acquisition

(SCADA) interface. To implement load-following capability, load measurements must be sent to the battery control system in real time. While this would be relatively straightforward in an industrial setting, such as a factory using energy storage to shave local peaks, integration with an existing utility SCADA system is more complex, as illustrated in Figure 2-2.

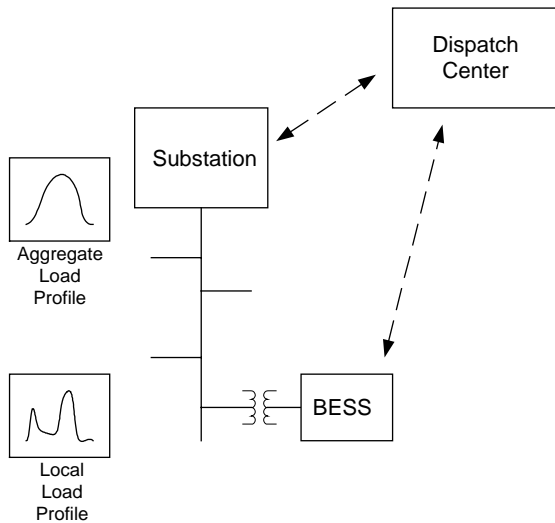


**Figure 2-2. Control over existing utility SCADA communications network.**

While the BESS could be placed at a distribution substation, it would in general be sited near the end of the distribution line so that benefits associated with line support could be captured in addition to relieving substation loads. However, dispatch of the battery would be based upon loading at the substation, which may be several miles away. While basing output control on local line loading would be easy to implement, these loads could differ significantly from aggregate substation loads, as illustrated in Figure 2-2.

Instead of installing communications directly between the substation and the battery, it was believed that the design should revolve around the existing SCADA infrastructure—including telecommunications equip-

ment and substation load sensors—as a cost-saving measure.

With this assumption, the utility dispatch center becomes the focal point of the communications scheme, and the essential BESS control design problem is integration with the SCADA network. Low-level protocols are defined by the network, and these may be programmed into the BESS with little effort, and the BESS becomes a node or remote terminal unit (RTU) on the network.

The more difficult question, however, revolves around where to place the intelligence of the battery control, that is, the logic to command specific real-time dispatch levels. In theory, the dispatch center would be the logical choice, because all of the distribution system information is collected there and the operators reside there.

However, the difficulty in implementing custom control programming into the proprietary SCADA system seemed to be an overriding factor, and it was established as a design goal to minimize the operator input requirements and, to the extent possible, place real-time control at the remote BESS. This approach was consistent with interviews of PG&E operators who desired to minimize attending the BESS, which would be operated during peak load times when operators have many demands competing for their attention.

The final SCADA design gave the dispatch operator controls to fix operating modes, including shutdown, block loading, and load following. Load following involved a one-time setup of a power threshold—above which the battery would discharge—and routing of real-time load data to the remote RTU.

The existence of a PC-based SCADA system (developed in-house by PG&E software developers as a low-cost alternative to the VAX platform) enabled Omnion to develop and test the SCADA interface. This SCADA version was used exclusively in the PG&E testing (see Appendix A for a more detailed description of the SCADA system design).

This page intentionally left blank.

### 3. Thermal Regulation

It is a well-established characteristic of lead-acid batteries (Linden, 1984) that operating temperature has a direct bearing on useful service life. Grid corrosion is accelerated at elevated temperatures, increasing internal electrical resistance and ultimately causing battery failure.

On the other hand, storage capacity (or ampere-hour capacity) increases with operating temperature. Higher capacities result in capital cost savings by reducing the number of batteries in the system and by reducing indirectly the balance-of-system cost (for example, the cost of the system enclosure is reduced for a physically smaller system).

The system designer, therefore, seeks to maintain battery temperatures within prescribed operating limits (generally between  $-10$  and  $40^{\circ}\text{C}$ ). In some cases, thermal design specifications can be met by circulating ambient air, particularly when the system is installed within a controlled environment.

In many cases, such as the PM250 prototype, fully integrated heating, ventilation, and air conditioning (HVAC) support systems are required to maintain thermal limits under wide ranges of external environmental conditions. The cost penalty of thermal regulation is recovered through extended economic system life and through capital and maintenance cost savings by avoiding battery replacements.

In addition to temperature-related performance impacts, the PM250 testing experience revealed that temperature differences between batteries of a given string are also an important design issue. As discussed below, temperature gradients were initially responsible for significant performance variations among batteries, and the air flow design was changed accordingly. Thus, the HVAC system is designed not only to maintain battery temperatures, but also to minimize temperature variations between batteries.

#### Data Acquisition

Container- and module-level parameters were monitored and reported to the SCADA system through an on-board monitoring computer. This computer was programmed to communicate using utility protocols, effectively acting as an RTU. In addition, two mod-

ules were independently monitored for individual battery voltages and temperatures, and this data was collected through a standard utility-grade RTU. See Appendix A for a complete description of the data acquisition system.

Data related to the thermal behavior of the system primarily came from Module 1 and Module 8 in Figure 3-1. These modules each contained 48 batteries in four tray "levels." Voltage measurements were taken across each 12-V battery terminal, providing a means to view detailed distributions of voltages under various conditions. In addition, each module included eight temperature measurements (thermocouples bonded to the battery walls) at the positions indicated.

Two voltage taps (one in each module) turned out to have poor electrical connections, preventing direct voltage measurements of four batteries. These voltages were therefore estimated in real time, and the analysis includes these estimated values.

One temperature measurement (on the edge of the second level in Module 1) was determined to provide erroneous data, and values from this thermocouple were excluded from this analysis.

#### Temperature Distributions

As reported previously (Ball, 1994), discrepancies between individual battery temperatures were observed during the course of testing the prototype PM250.

Figure 3-2 shows the string voltages for Modules 1 and 8 during two 40-minute block load tests on November 17, 1993, and February 21, 1994. These curves include the characteristic drop in voltage at the initiation of the discharge (corresponding with internal resistance) and show the gradual voltage decay as the battery drops in state of charge over the discharge period.

The battery temperatures taken from Modules 1 and 8 corresponding to these tests are shown in Figure 3-3. The first chart indicates that battery temperatures varied by as much as  $5^{\circ}\text{C}$ . The second chart shows the same measurements after modifications to the air

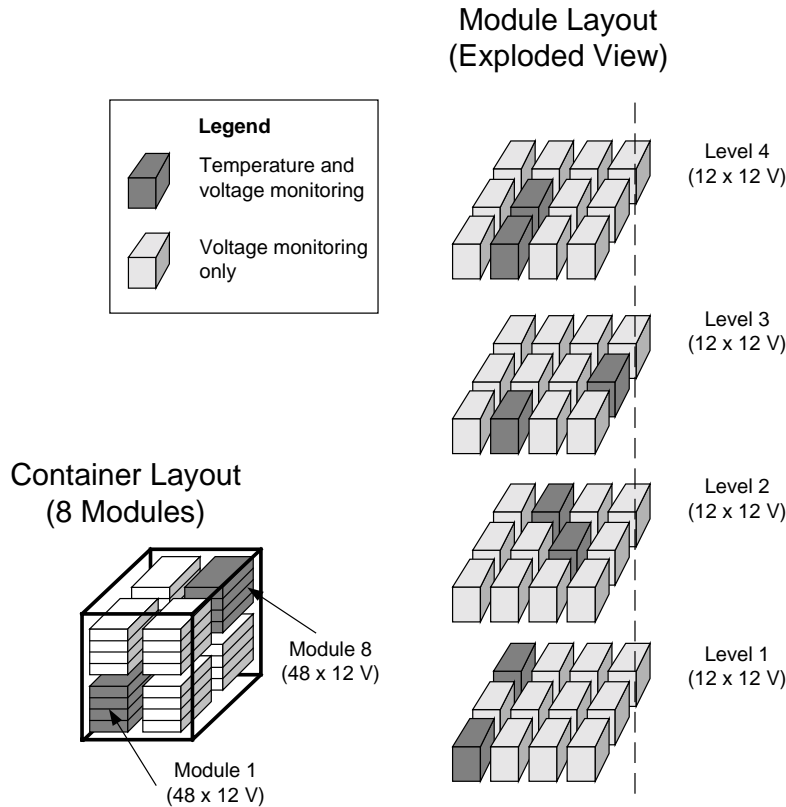


**Figure 3-1. Module and container layouts.**

flow design were implemented in the container, reducing the variation to under 3°C.

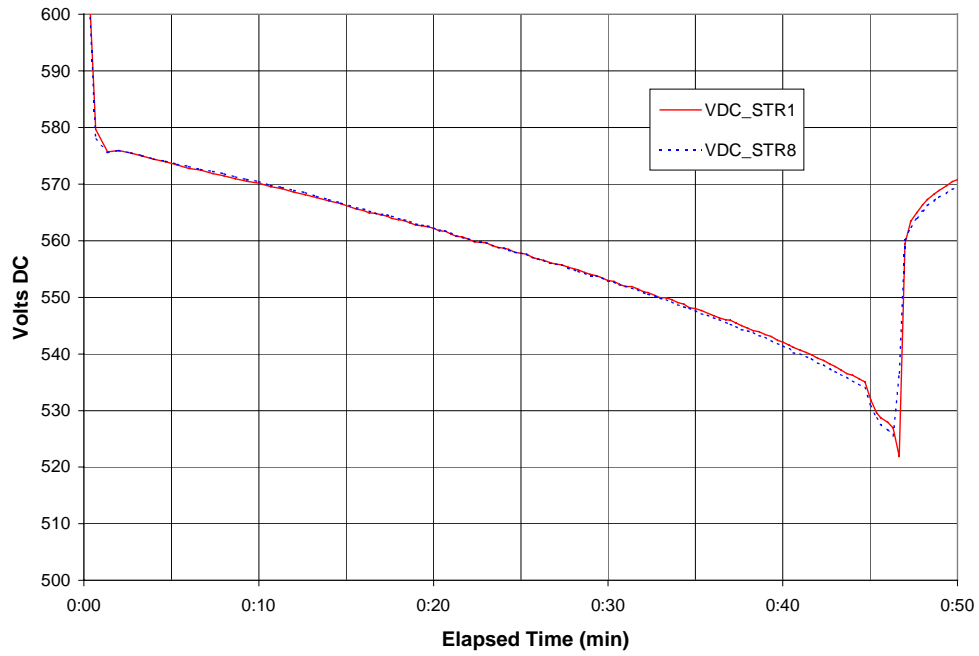
Air flow modifications were introduced based on field observations similar to those illustrated in Figure 3-4. These charts show average discharge temperatures for individual batteries during the two tests. Because one of the roof-mounted air conditioners came on about 34 minutes into the second test (which can be seen in Figure 3-3), only samples taken during the first 30 minutes of the respective tests are averaged and included in the charts. Several observations may be made based upon these results:

1. Temperatures in Module 8 were initially higher than those in Module 1. Module 8 was located among the top modules in the container, whereas Module 1 was among the bottom modules. This arrangement suggests that temperatures may have been influenced initially more by air buoyancy in the container rather than by forced circulation.

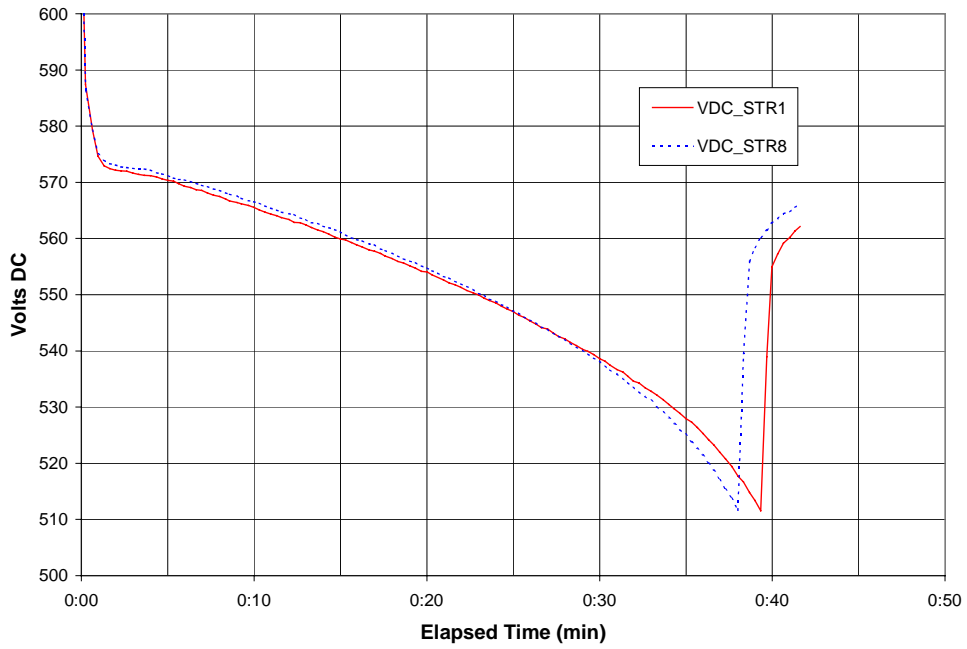
2. Thermal gradients initially existed within modules, with hotter batteries located on the upper trays and cooler batteries on the bottom trays. This was particularly true in Module 1, possibly due to poorer circulation of air in the bottom of the container.
3. Both of the two thermal trends identified above seemed to be eliminated by the air flow modifications. As shown in Table 3-1, temperatures were observed within a significantly narrower range in the later test.

**Table 3-1. Battery Temperatures During 40-minute Discharge Tests**

Test Date	Mean Battery Temperature (°C)	Standard Deviation (°C)
11/17/93	22.2	1.42
2/21/94	20.2	0.60

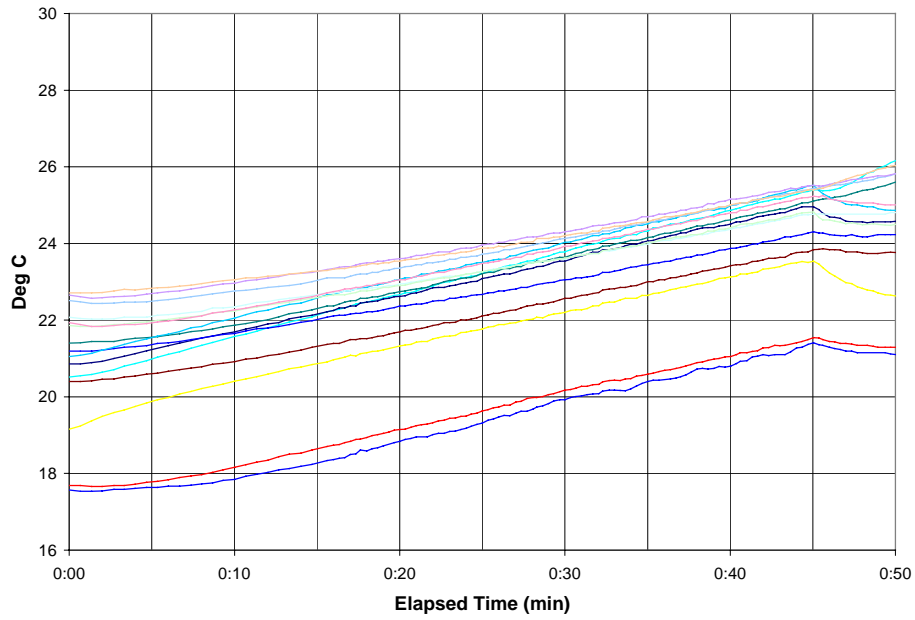


(a)

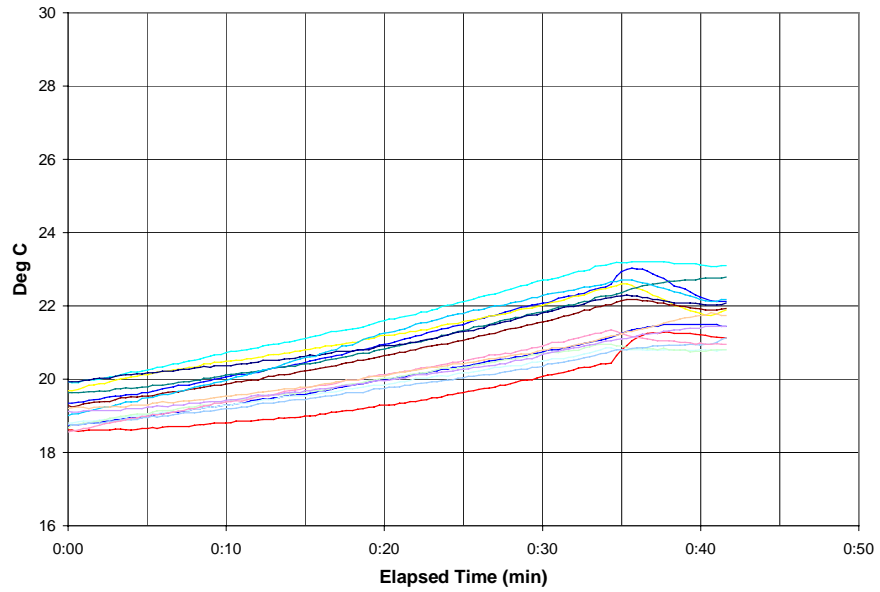


(b)

Figure 3-2. String voltages for Modules 1 and 8 during 40-minute discharges on (a) November 17, 1993, and (b) February 21, 1994.

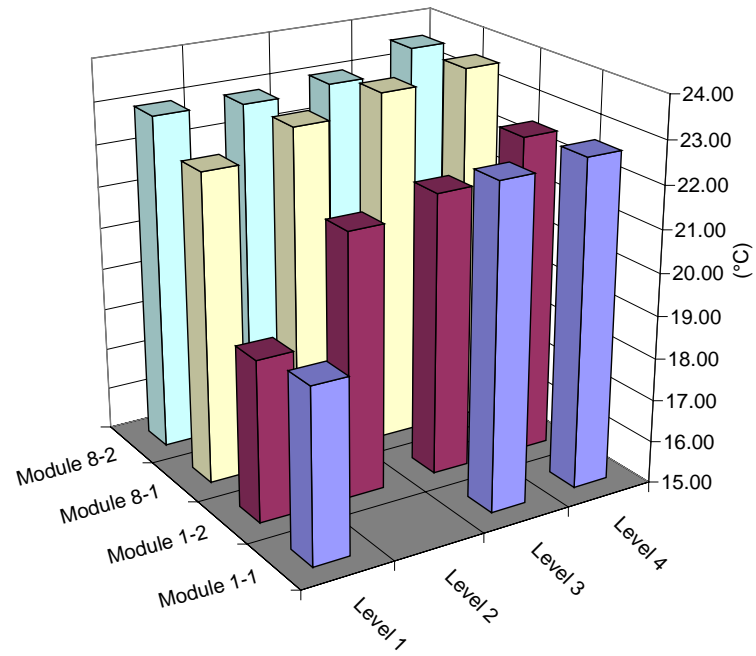


(a)

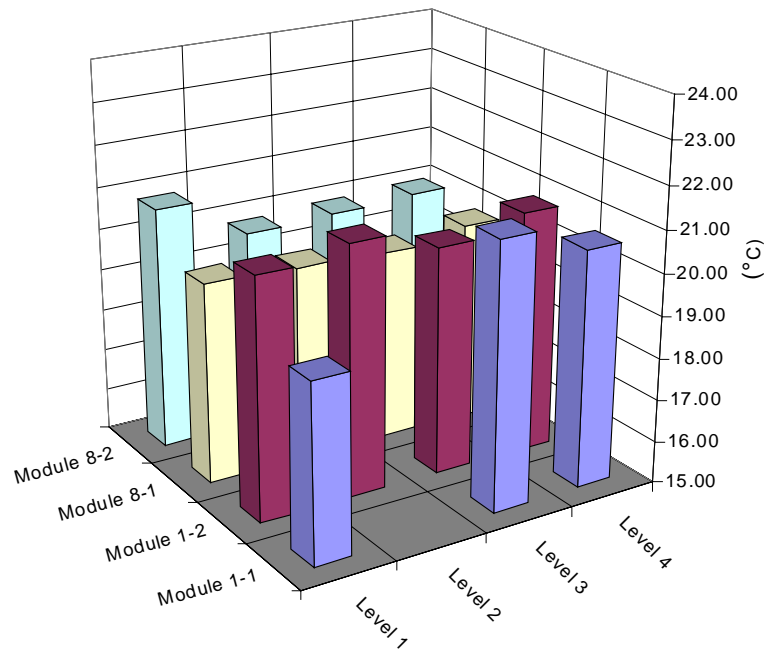


(b)

Figure 3-3. Battery temperatures during 40-minute discharges on (a) November 17, 1993, before air flow modifications, and (b) February 24, 1994, after air flow modifications.



(a)



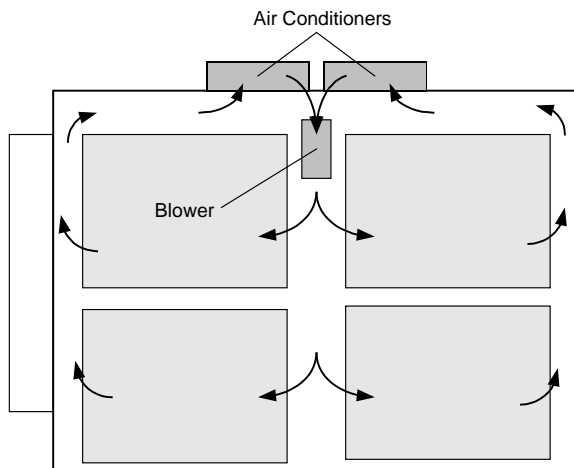
(b)

Figure 3-4. Average battery temperatures on (a) November 17, 1993, and (b) February 21, 1994.

## Air Flow Design

Air flow design modifications included (1) the addition of a high capacity blower, (2) installation of baffling between modules and container walls, and (3) varying module air inlet cross sections.

The blower was a 2000/1500 cubic-feet-per-minute (CFM) two-speed model, set on the high speed. The blower was placed in the central top region of the container, and oriented such that the air discharged down into the central container, as shown in Figure 3-5.



**Figure 3-5. Forced air circulation scheme in PM250 prototype container, after modifications.**

To prevent air from circulating between the modules and the container walls (bypassing the batteries in the modules), baffling was installed to block this flow. Air was drawn through the modules by a fan in the power conditioning section of each module, and it was returned to the top of the container between the ends of the module and the end walls of the container. The inlet to the air conditioner (when turned on) was therefore the warm air discharged from the modules.

To counteract the thermal gradients within the modules, air inlets were modified by increasing the inlet cross-sectional area on the upper trays relative to the lower trays. This provided for slightly greater air flow on the upper trays, as illustrated in Figure 3-6.

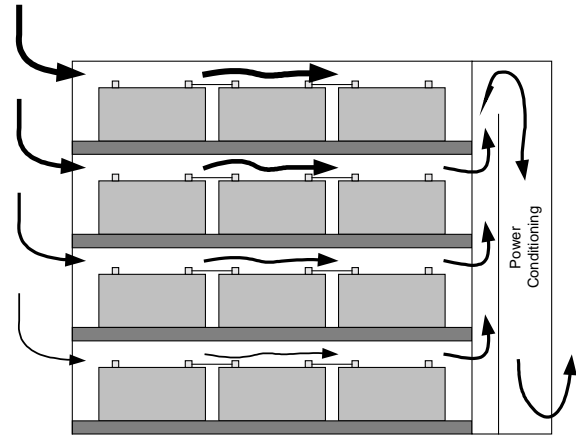


**Figure 3-6. Air circulation within the modules.**

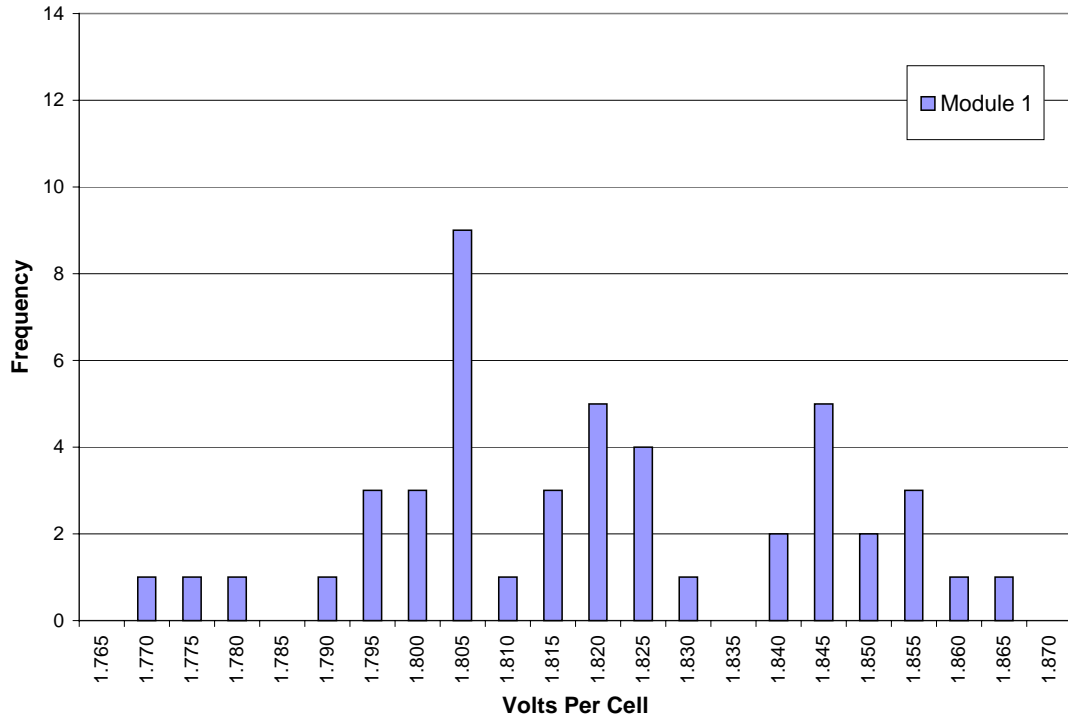
## Temperature Impacts on String Voltages

Data collected from the 40-minute discharge test on November 17, 1993, provide a means to study the impact of temperatures on string behavior, in particular the variations of temperature within a string.

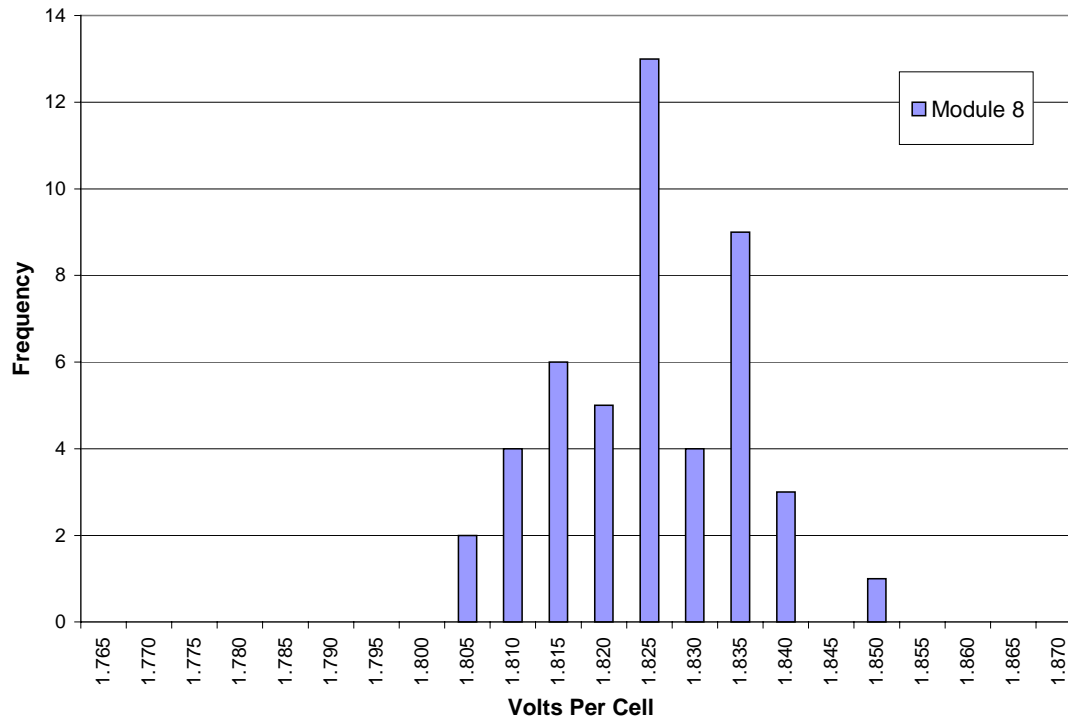
Figure 3-7 illustrates the impact of temperature variability in end-of-discharge (EOD) voltages. The charts show individual battery voltages taken for Modules 1 and 8 immediately before the completion of the discharge, corresponding to the minimum string voltage in Figure 3-2(a), at approximately 47 minutes of elapsed time. Module 1, with the high thermal variation across the string, shows a significant range in EOD voltages relative to Module 8. Because the data were taken during the same test and under the same loads, the results suggest that temperature differences are responsible for the differences in voltage distributions.

Indeed, the relationship between battery temperatures and EOD voltage distribution is shown in Figure 3-8. These charts, which show average discharge temperatures over the full 40-minute discharge, indicate a very strong relationship between these variables for Module 1, which has a wide range of temperatures. Module 8, representing a string in a more controlled thermal environment, indicates a tight range of temperatures and voltages.

A regression analysis was performed on Module 1, for which a reasonable range of average temperatures was available, and the correlation was shown to be 86.2%. Regression coefficients and other statistical

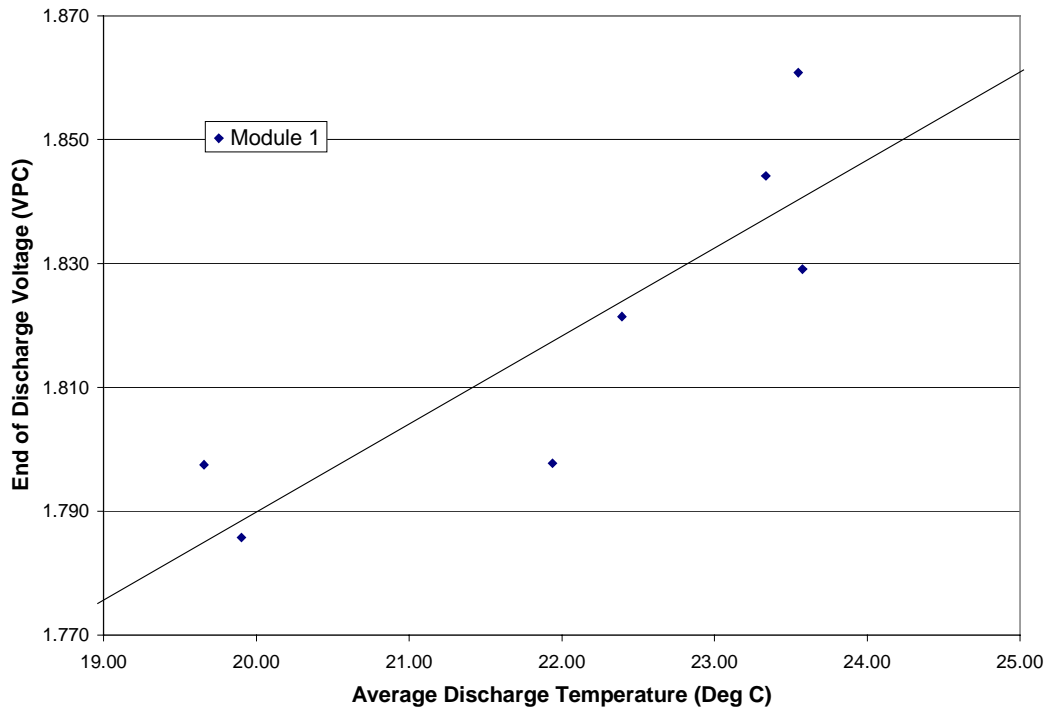


(a)

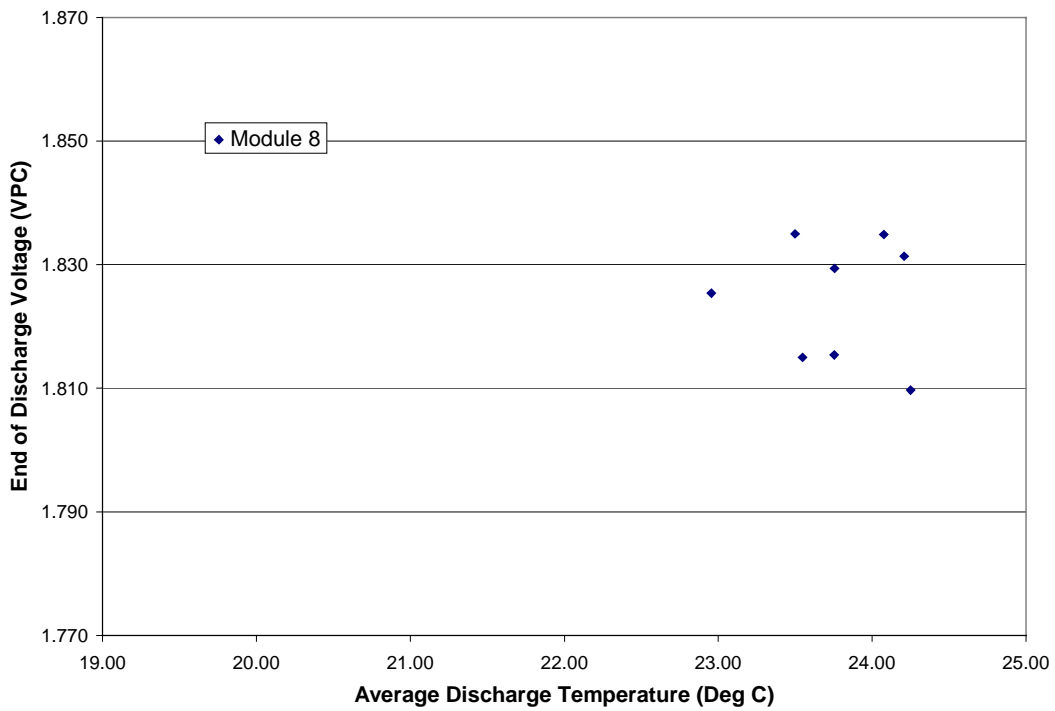


(b)

Figure 3-7. End-of-discharge voltages on November 17, 1993, for all 48 batteries in (a) Module 1 and (b) Module 8.



(a)



(b)

Figure 3-8. Relationship between EOD voltage and average discharge temperature for (a) Module 1 and (b) Module 8.

results are shown in Table 3-2, and the least-squares curve fit is shown in Figure 3-8(a).

**Table 3-2. Regression Statistics Showing Correlation Between Average Discharge Temperature and EOD Voltage**

Multiple R	0.862
R Square	0.743
Adjusted R Square	0.692
Standard Error	0.0152
Observations	7
Intercept	1.507
X Variable 1	0.01416

The relationship between voltage and temperature is further understood by viewing the EOD voltage distributions by tray level, illustrated in Figures 3-9 and 3-10. EOD voltages in Module 1 clearly are higher in the upper trays where temperatures are elevated. On the other hand, EOD voltages in Module 8 are not strongly related to tray level.

In the PM250 prototype, electrical connections were made such that string voltages were made of series connections within and between trays. Connections between trays were in order of tray level (Tray 1, Tray 2, etc.). The negative half of the string corresponded with the bottom two trays, while the positive half corresponded with the upper two trays.

Thus, a voltage imbalance between the positive and negative strings must have developed as a result of the temperature imbalance.

String imbalance was identified during the course of testing as an indicator of the health of the string (see Chapter 4 for a more complete discussion). An independent measurement related to voltage imbalance was taken and recorded in the data set, and this measurement is shown in Figure 3-11 for Modules 1 and 8. As expected, the imbalance in Module 1 is substantial, whereas the imbalance in Module 8 is not as significant.

## Temperature Impact on Capacity

With a clear relationship between EOD voltage and discharge temperature established, it is of interest to determine the impact of temperature imbalance on string behavior over the entire discharge period, not only at the end of discharge. Specifically, we wish to investigate energy storage capacity as a key measure of string performance.

Discounting small effects of ground leakage current, all cells in a given string share the same current during charge and discharge. The energy capacity, which is discharged by a given cell, is therefore calculated from the string current and the cell voltage as

$$C_{cell} = \int i_{str}(t)v_{cell}(t)dt,$$

where the integration is performed over the duration of the discharge. While this calculation could be made over the charging interval as well (which would provide round-trip efficiencies), the data collected were not sampled at a rate fast enough to adequately match changes in voltage and current seen during the manufacturer's proprietary charge regime at the top of charge.

The results are plotted in Figure 3-12, which correlates cell capacities versus average temperatures from Module 1. The relationship is seen to be similar to the EOD voltage curve, indicating that relationships between cell voltages are preserved over the course of the discharge.

The curve indicates that warmer batteries in the string—those in the upper trays in the PM250 prototype—discharge more energy than cooler batteries. These batteries, therefore, must have received more charge during the charging portion of the cycle. It is expected that the imbalance in cell state of charge is ultimately harmful to the weaker cells in the string and would cause premature failure. Premature failure may be of particular concern when strings are connected in parallel (unlike the PM250).

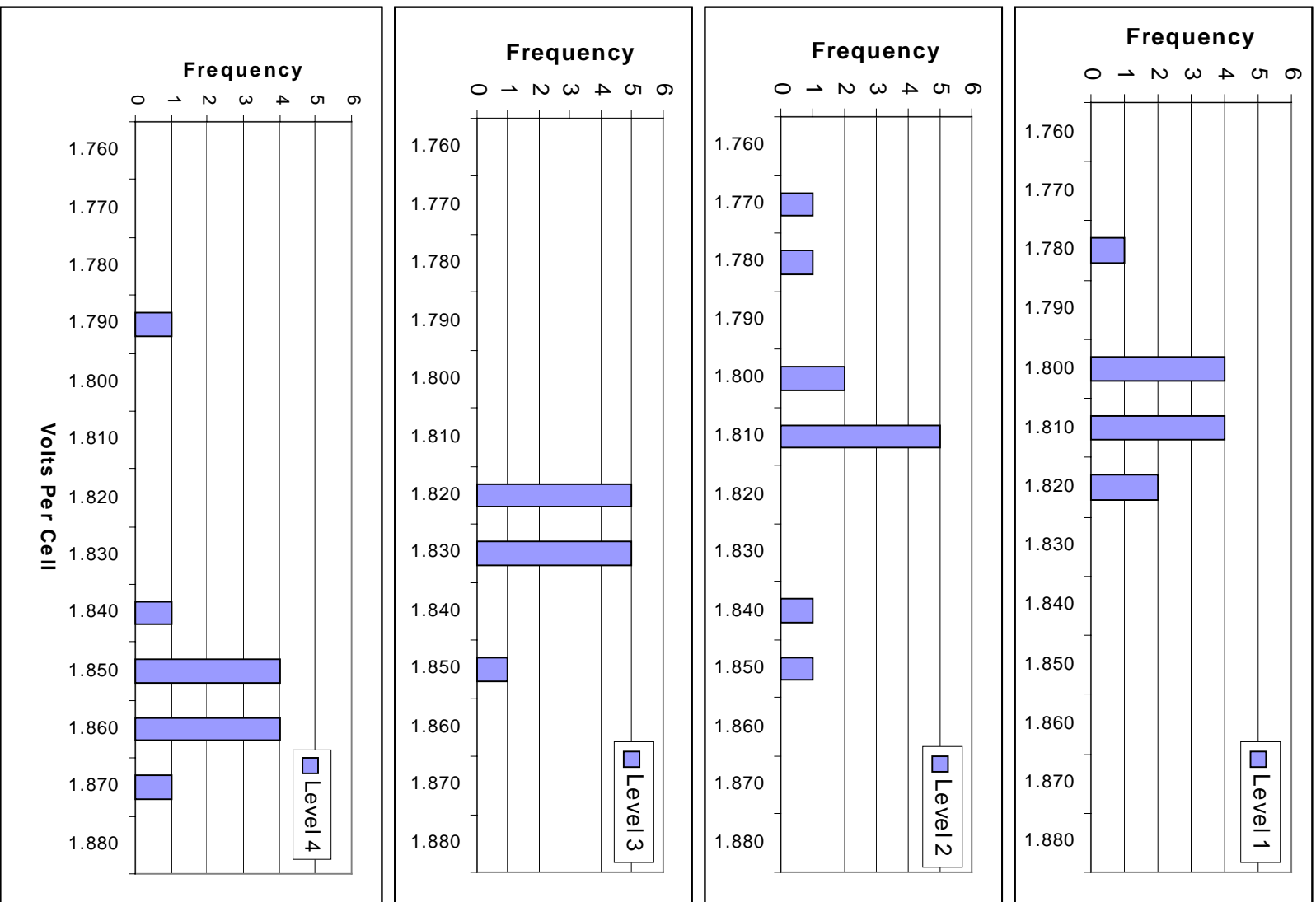


Figure 3-9. Distribution of Module 1 EOD voltages by tray level.

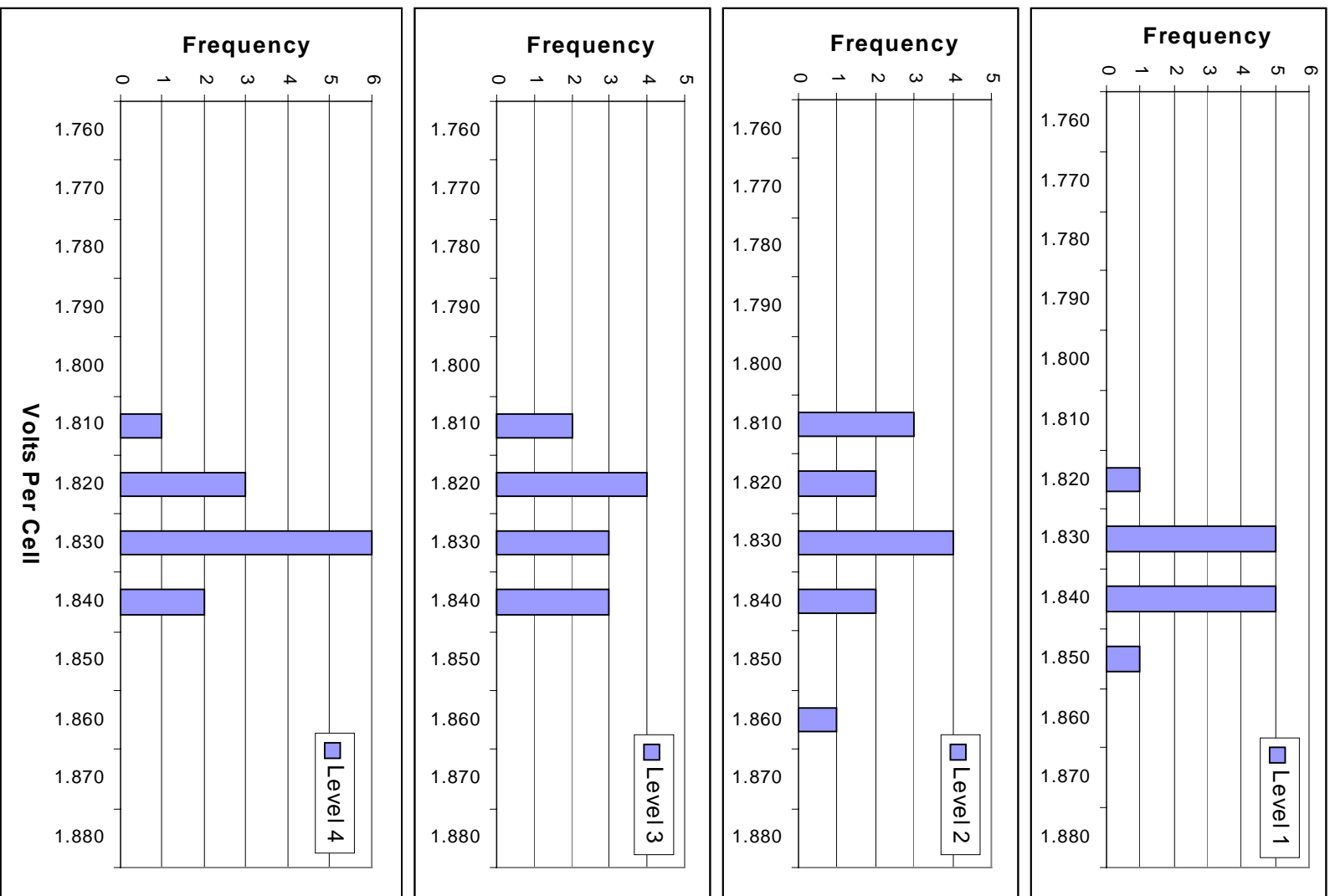


Figure 3-10. Distribution of Module 8 EOD voltages by tray level.

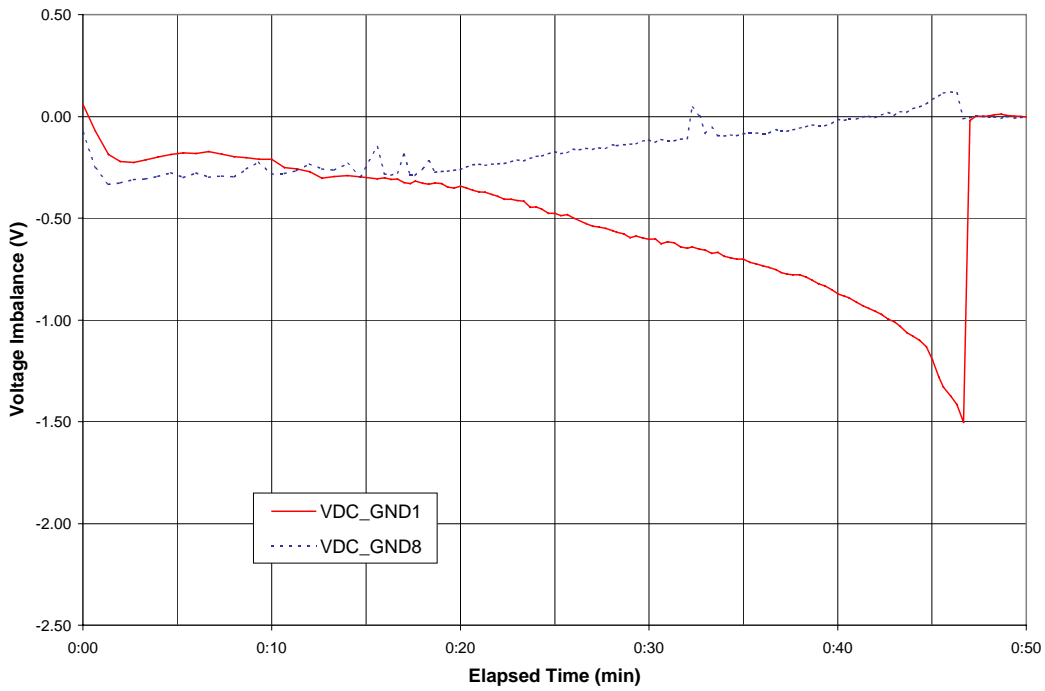


Figure 3-11. String imbalance for Modules 1 and 8 during 40-minute discharge.

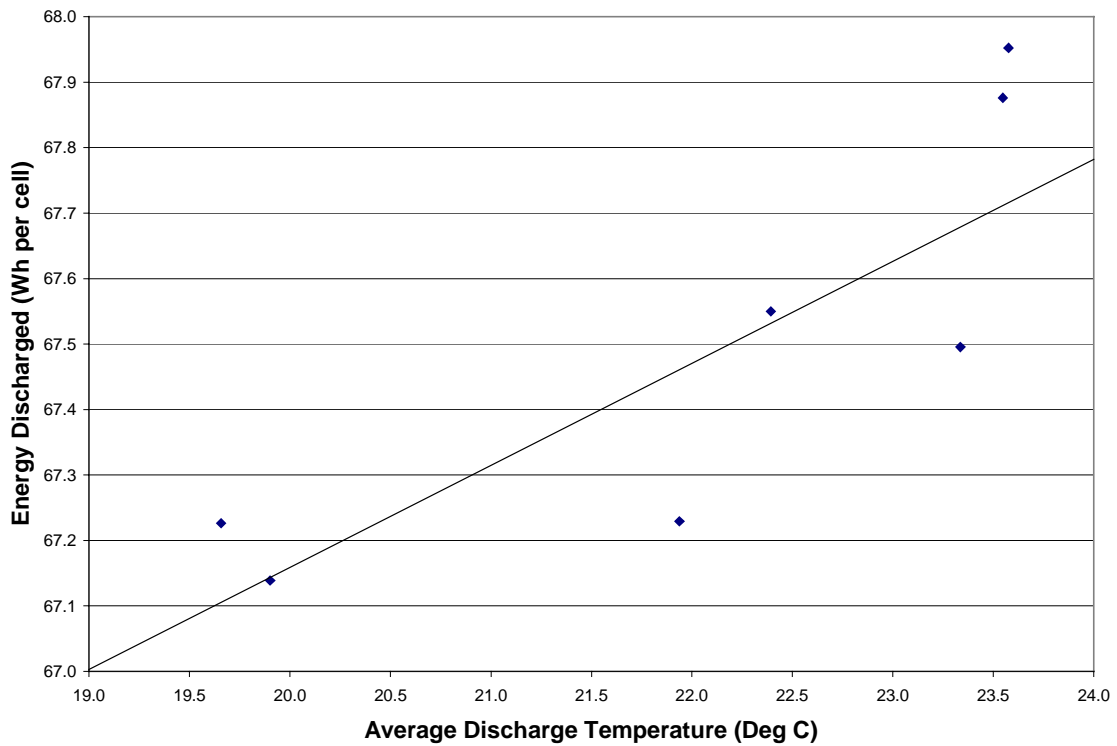


Figure 3-12. Cell capacity versus average discharge temperature.

## 4. End-of-Life Prediction

Battery replacements are expected to be a routine activity for grid-connected BESS applications and a significant contributor to life-cycle cost. Battery replacements involve capital outlays for new batteries, shipping and disposal fees for old batteries, and labor costs to remove and replace batteries in the enclosure. Consequently, it is of interest to be able to predict battery EOL in order to

- maximize the useful life of the batteries
- prevent unnecessary replacements
- avoid costly downtime
- schedule replacements in coordination with other maintenance activity

While battery design optimization and EOL estimates can be made readily with established float and automotive applications, accurate EOL prediction methodologies for deep cycle applications such as BESS have remained elusive. In these cases, EOL prediction is complicated by inadequate understanding of the impacts of depth of discharge, variable discharge rates, frequency of cycling, fluctuating operating temperatures, and charging methods.

### String Failure

It is generally accepted that individual cell failures within a string permit continued operation because cells in lead-acid batteries fail in the shorted condition, for example, the string continues to conduct current (at reduced capacity) with shorted cells. Only after several cells fail in a given string does the string capacity degrade to a state considered to be the end of life.

Individual cell failures therefore provide a convenient diagnostic foundation for predicting impending string failure. While the impact of individual cells is unique to each string design and battery make, the knowledge of failed cells can broadly be applied as an indicator of near-term string failure.

### Goal of Analysis

In light of the above discussion, we seek to develop a methodology for predicting battery string EOL based on the determination of premature cell failures.

An EOL indicator should ideally be based on simple measurements and straightforward statistical analysis. Manufacturer life-cycle performance data is insufficient for this purpose because it assumes consistent rates and depths of discharge under specific operating conditions; these data are of little use in most utility energy applications. The technique should be

- *Easy to measure/calculate* – It should require few intrusive monitoring devices, avoid electrochemical modeling, and provide simple numerical or graphical signals to the existence of an arising problem.
- *Easy to communicate* – It should be easily understood by end-users who will ultimately use the results to make decisions about battery replacements.
- *Accurate* – It should definitively indicate the state of health of the string. It should provide results that do not vary with external conditions.
- *Repeatable* – It should provide consistent and reliable conclusions.

### Voltage Imbalance

#### Discovery of Failed Batteries

Two of the eight modules (Module 1 and Module 8) in the prototype PM250 system were monitored for individual voltages on each of the 48 batteries. This gave researchers the ability to closely watch the behavior of the strings, and to detect any single battery problems that might occur.

The measurements led to an early discovery of defective batteries in Module 1. Figure 4-1 shows a plot of the average battery voltage and that of a single failed battery in Module 1 during a baseline test performed at the manufacturer's facility. The baseline test consisted of a discharge for over an hour at approximately 167 kW. The voltage across battery #15 shows a dramatic departure from the string average, and drops to below 9.0 V at the end of discharge.

A subsequent baseline test performed shortly after the system arrived at PG&E revealed similar behavior in battery #15 and in battery #16. Plans were made to replace these batteries before continuing with qualification tests.

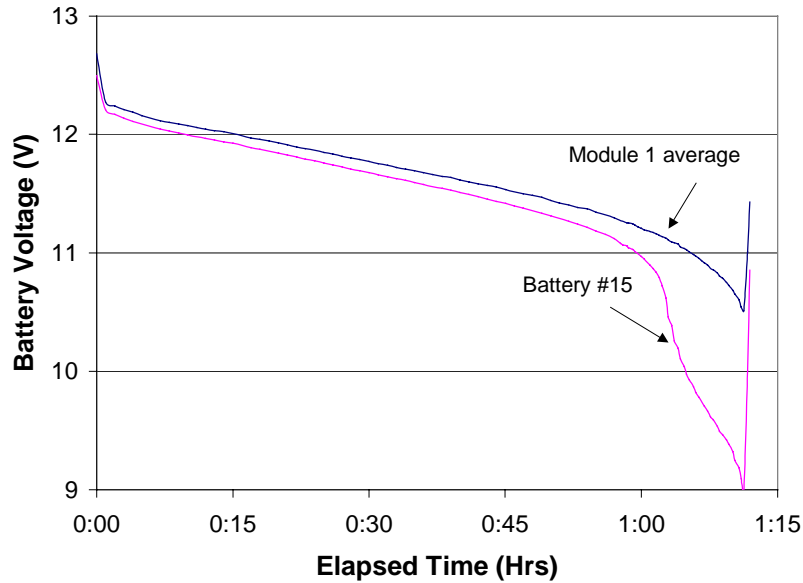


**Figure 4-1. Module 1 average battery voltage and failed battery voltage during early qualifying tests.**

The shape of the voltage drop that occurred in the two batteries during the baseline discharge also appeared in the string imbalance voltage measurement of Module 1. This measurement was designed to detect ground faults in the DC string, but also provided an indication of the voltage difference between the top and bottom half of the module string. In ideal string conditions, this value should be zero, but several factors cause discrepancies between the two. Clearly one such factor is a failed battery in one half of the string.

Because the imbalance voltage was measured in every module, it was concluded that the detection of a similar profile might prove a convenient indicator for a failing battery or batteries. The supposition was validated with Module 3, as illustrated in Figure 4-2. This figure shows the imbalance voltage across all eight modules during the second baseline.

While not as dramatic as the drop in Module 1, the imbalance voltage in Module 3 displays the characteristic falloff that precedes the drop normally expected towards the end of a deep discharge. Module 3 was inspected when the batteries of Module 1 were replaced and was indeed found to have a defective battery. In tests immediately following the battery replacements in these two modules, the imbalance voltage profiles were similar to those of the other modules.

## Imbalance Voltage Measurement

The string imbalance voltage measurement is illustrated in Figure 4-3. The battery string feeds a parallel capacitor bus in the DC-AC converter. The total voltages across the battery string and capacitor circuit are the same, so that

$$2V = V_{\text{top}} + V_{\text{bot}}$$

The capacitor bus is center-point grounded and uses resistors to maintain balanced voltages across the top and bottom half. Therefore, any discrepancies between  $V_{\text{top}}$  and  $V_{\text{bot}}$  of the battery string creates a potential ( $V_{\text{imb}}$ ) across the grounding resistor. Therefore,

$$V_{\text{imb}} = V_{\text{bot}} - V$$

For example, if the total string voltage ( $2xV$ ) is 600 Vdc, then the capacitor bus maintains 300 Vdc on the top and bottom half. If  $V_{\text{top}} = 302$  Vdc, then  $V_{\text{bot}} = 298$  Vdc. The difference between  $V_{\text{top}}$  and  $V_{\text{bot}}$  is 4 Vdc, and the imbalance voltage  $V_{\text{imb}}$  is equal to  $-2$  Vdc ( $298 - 300$ ).

## Imbalance Voltage Characteristics

Repeated testing revealed that the imbalance voltage tends to drop over the course of a deep-cycle discharge, even if all the batteries are healthy. This can

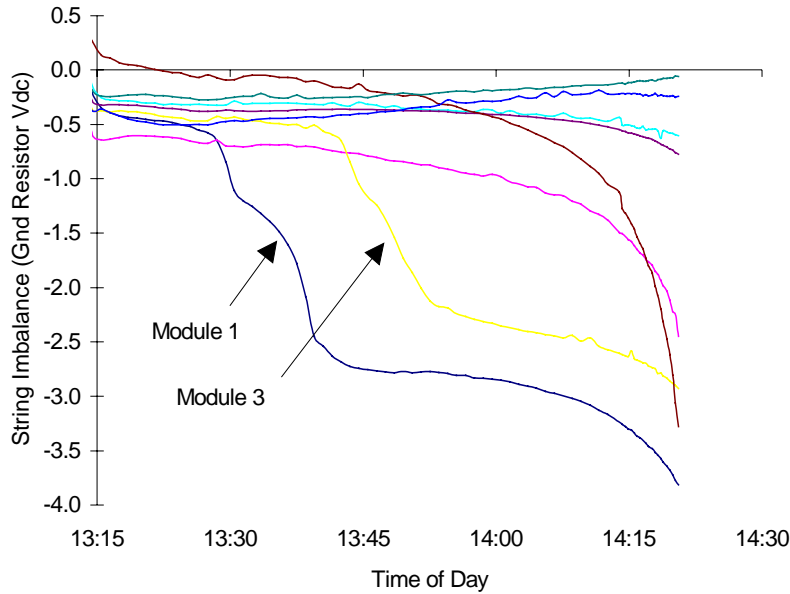


Figure 4-2. Eight string imbalance voltages.

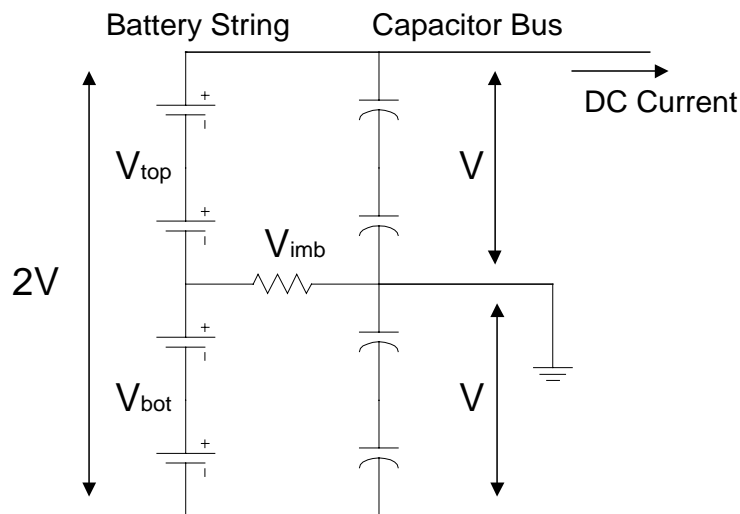


Figure 4-3. Voltage imbalance measurement circuit.

be seen in the imbalance voltages of Figure 4-2 described earlier. The phenomenon is attributed to the fact that the bottom half of the string, which is physically located on trays below the top half of the string, operates slightly cooler. Cooler batteries have less capacity than warmer ones, and therefore incur a greater voltage drop when supplying the same amount of current.

The impact of this tendency on using the imbalance voltage as a battery diagnostic tool is not consistent. If the failed battery or batteries are located on the bottom half of the string, the reduced voltage com-

pounds the drop over time, and is clearly apparent. A failed battery in the top half of the string, however, would tend to pull the imbalance voltage up, and offset the expected drop over time. As a result, no clear pattern in the imbalance voltage may emerge from such a case.

Furthermore, the detection of a failed battery on the bottom half of a string may be obscured if there is another failed battery on the top half. This phenomenon can be illustrated by the imbalance voltage measurements made in Module 1 during the latter portion of the test period. Figure 4-4 shows how the imbal-

ance voltage profiles change over these later baselines (after failed batteries #15 and #16 were replaced). While the voltage drops are significant towards the end of discharge, there is not a clear drop-off early in the discharge as was evident in the earlier case. However, the individual battery monitors in Module 1 revealed one battery (#43) that appeared to have failed, and another (#9) that was at the very least abnormally low, during the Baseline #6 test. These batteries are illustrated by the measured voltages shown in Figure 4-5. Note that the problem batteries are on either side of the mid-point voltage, each

counteracting the effect of the other in the imbalance measurement.

Despite these inconsistencies, the existence of failed batteries was detected from the imbalance voltage in at least two other modules over the course of testing. The imbalance voltage histories for Modules 2 and 3 are shown, respectively, in Figure 4-6. Module 2 shows pronounced problems in both Baseline 5 and especially Baseline 6, whereas Module 3 voltages show no clear problem until Baseline 6.

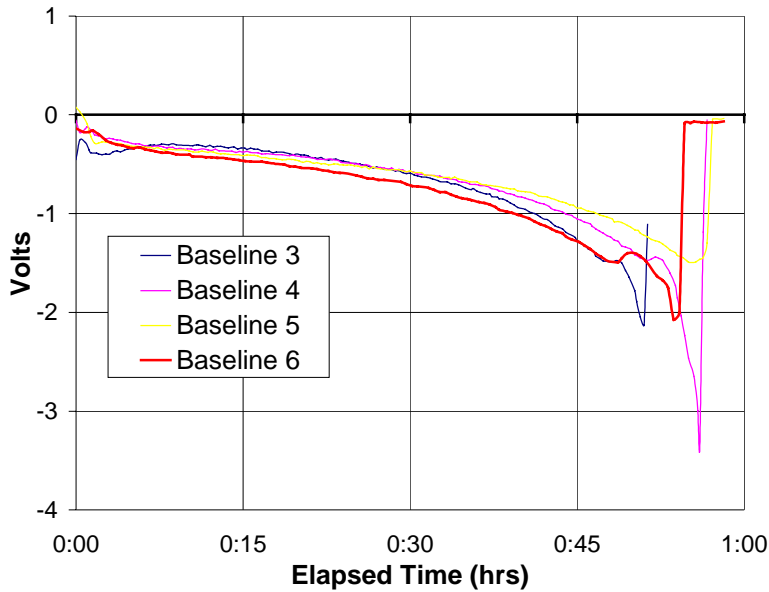


Figure 4-4. Module 1 imbalance voltages over the course of several baseline tests.

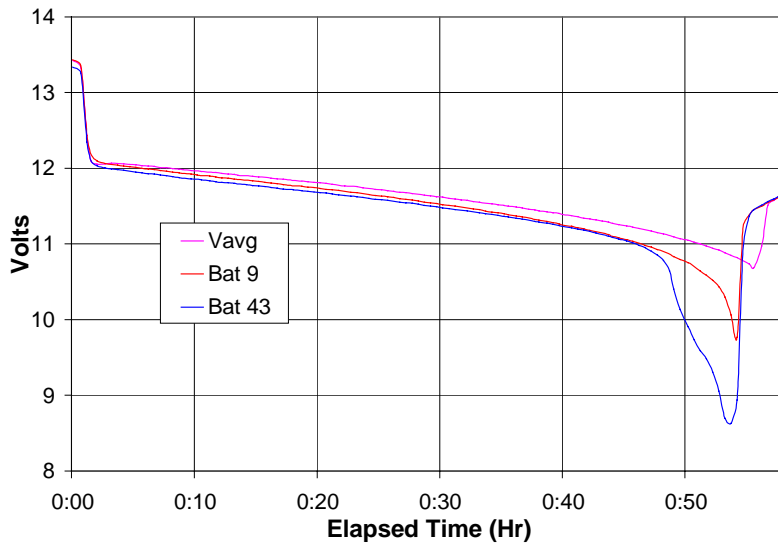
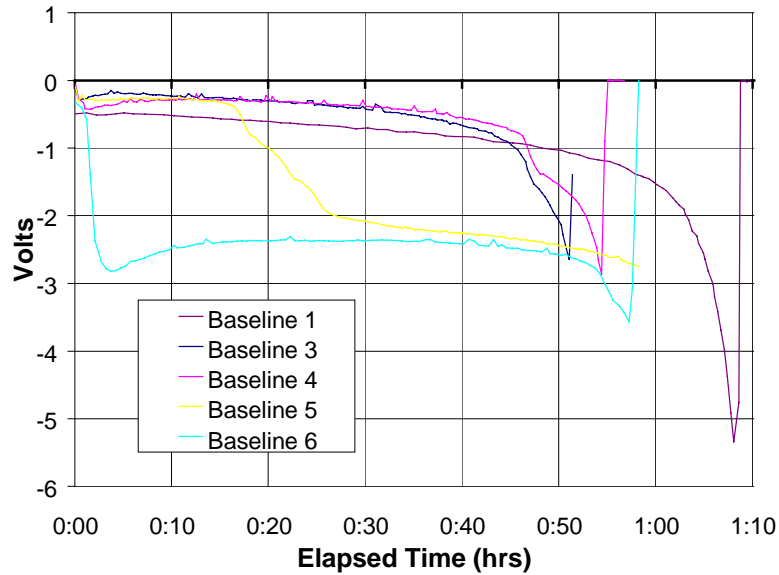
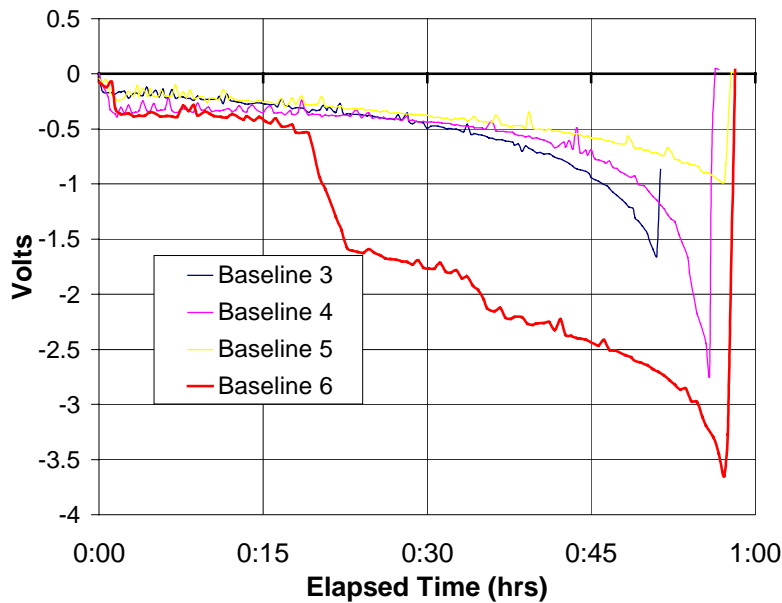


Figure 4-5. Module 1 average, battery #9 and #43 voltages during Baseline test #6.



(a)



(b)

Figure 4-6. Imbalance voltage histories for (a) Module 2 and (b) Module 3.

## Quarter-String Measurements

Dividing the string measurement into four quarters may significantly improve failure diagnostic capabilities in cases where a problem battery exists on both the bottom and top half of the string. Such a measurement requires only two additional monitoring channels per module. Currently, leads are attached to the bottom of the string, the top of the string, and at the positive terminal of battery #24. The extra two

leads would be connected to the positive terminal of batteries #12 and #36.

The usefulness of quarter-string measurements derives partially from the phenomenon described earlier in which the voltage on the bottom half of the string tends to decrease relative to that of the top half during a deep discharge.

The average battery voltage in the top half of the string should increase relative to the average of the entire string, while the average on the lower half of the string should decrease proportionally.

Figure 4-7 illustrates this voltage effect. The lines labeled Q1 through Q4 represent the difference between the average battery voltage in each corresponding quarter string and the total string average. Specifically,

$$\begin{aligned} Q1 &= V_{Q1}/12 - V_{\text{string}} / 48, \\ Q2 &= V_{Q2}/12 - V_{\text{string}} / 48, \\ Q3 &= V_{Q3}/12 - V_{\text{string}} / 48, \text{ and} \\ Q4 &= V_{Q4}/12 - V_{\text{string}} / 48, \end{aligned}$$

where

$V_{Q1}$  = the voltage measured from battery #12 to the bottom of the string,  
 $V_{Q2}$  = the voltage measured from battery #24 to battery #12,  
 $V_{Q3}$  = the voltage measured from battery #36 to battery #24, and  
 $V_{Q4}$  = the voltage measured from the top of the string to battery #36.

So, while Q1 and Q2 drop with respect to the average, Q3 and Q4 increase. The sum of all four at any given time should ideally equal zero.

Figure Fig. 4-7 shows the quarter-string averages as they deviate from the total string average in Module 1 during the factory baseline test. Note the pronounced drop in Q2 (batteries 13 through 24), which, from the intensive monitoring, is known to be caused by the failure of battery #15. There is also a slight decay in Q4, an early indicator of the deterioration of battery #43.

Figure 4-8 shows the same measurements in Module 1 during Baseline 6 (after failed battery #15 was replaced). As described earlier, this test revealed nothing conclusive from the imbalance voltage, presumably due to the existence of problematic batteries on both the top and bottom half of the battery string. The quarter strings shown here, however, reveal a clear failure in Q4 (known to be battery #43), and a potential failure in Q1 (known to be battery #9).

## Additional Considerations

The use of quarter-string measurements may significantly improve the detection of failed batteries in a string. Voltage imbalance is shown to be an indicator of failed batteries, but under some conditions may be unreliable.

The quarter-string technique is a more reliable indicator of failed batteries because double cell failures can be detected and isolated in the quarter strings. Only in the condition that each quarter string contains the same number of failed cells would the problem go undetected, but the probability of this occurring is expected to be very small because the failure would be noticed before the condition ever occurred.

Other factors may obscure the diagnosis, such as the distribution of batteries that have not yet failed but are operating at lower than average voltages. Even in these cases, however, failed batteries should reveal themselves if their voltage drop shows up sufficiently early in the discharge period.

It is important to note that batteries failing within the PM250 module strings do not cause outright module or system failures. The cell failures and reversals fail as a short, thus allowing current to continue flowing through the string. Their existence shortens module life by compounding imbalances in the batteries' state of charge and accelerating the occurrence of voltage-cutoff violations at the end of a discharge.

In the case of the PM250, cell failures may cause a more immediate loss of a module if imbalance voltages exceed ground fault limits. Apart from the predictive indicators described in this section, other general indicators of a module's ill health were revealed during the PM250 testing. Most notable is the total string voltage at the beginning and end of discharge. Modules with consistently lower voltages at the beginning of a discharge were unable to receive adequate charging. This type of pattern typically emerges far in advance of the module reaching its defined EOL capacity.

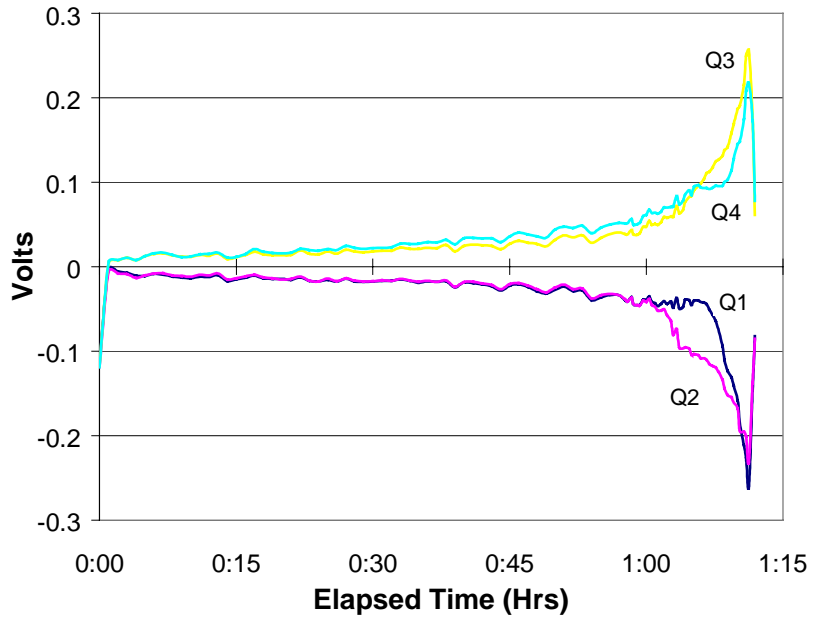


Figure 4-7. Module 1, Baseline 1; Average battery voltage in each quarter string relative to string average.

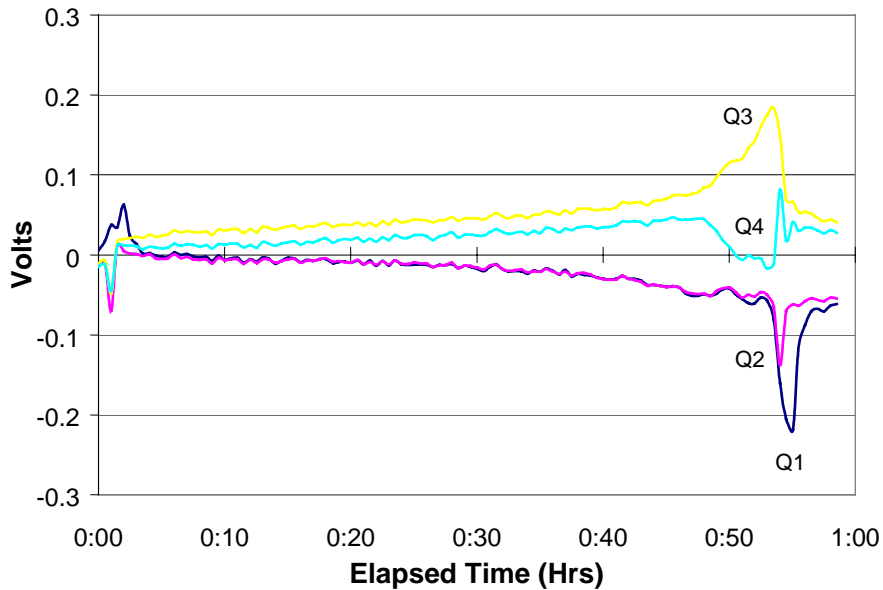


Figure 4-8. Module 1, Baseline 6; Average battery voltage in each quarter string relative to string average.

This page intentionally left blank.

## 5. Conclusions

The experience with the PM250 was an excellent opportunity to address many system-level issues faced by designers of grid-connected BESS systems. Most of the issues uncovered during testing are applicable to energy storage systems in general, not only to the PM250 design. The key conclusions are discussed below.

### Battery Technology

System designers face a difficult choice in the selection of battery technologies. For long storage applications, batteries account for a significant portion of the overall capital cost, and the reliability of the system is largely driven by performance of the batteries over many cycles. Low-cost automotive or marine batteries exist in high production volumes, but their low cycle lives require that batteries be replaced on a regular schedule, driving up system life-cycle costs. Advanced battery technologies may be able to meet cycling, cost, and energy density requirements of BESS market constraints.

### Charge Control

The battery designers of the prototype PM250 implemented novel charging methods that were intended to enhance cycle life and system reliability. Such charging methods are now possible through fine control of advanced integrated gate bipolar transistor power conditioning systems. While we lack a solid understanding of the effects of such charging methods, it appears that BESS systems will benefit from this approach.

### Utility Protection

Each utility has rigorous interconnection requirements that must be met by the BESS designers as a condition of connecting to the grid. While the requirements are generally well defined for rotating generators found at independent power producers and cogenerators, utility protection engineers have begun only recently to address protection schemes involving solid-state inverters and power conditioning equipment.

Traditionally, protection has been accomplished with mechanical relays. However, BESS systems are generally capable of meeting requirements through the use of solid-state controls, and the acceptance of these devices by utility engineers will be important for the widespread introduction of BESS into the utility environment. Some photovoltaic inverters have been pre-approved by utilities, and it will be important for BESS manufacturers to follow this approach. Pre-approvals will lower the overall installation cost since utility protection engineers will be familiar with the equipment and will not have to re-view each BESS installation on a case-by-case basis.

### Load Following

“Smart” dispatch strategies such as load following enable peaks to be met with minimal battery hardware investment. However, the communications schemes required to implement load following in a utility environment are complex, and implementation requires some customization for compatibility with existing SCADA infrastructure.

### Thermal Regulation

Thermal regulation turns out to be a major factor in the performance and reliability of the BESS system. The HVAC system must be designed to maintain overall battery temperature limits and must minimize thermal gradients within series-connected strings.

Thermal gradients in the PM250 battery container and within modules necessitated air flow modifications, including the addition of a high-capacity blower and changes to the air flow pathways to increase overall air circulation and improve convective heat transfer.

### End-of-Life Prediction

It is highly desirable to be able to predict battery EOL in order to facilitate battery replacement scheduling and avoid downtime. However, measurement of individual battery voltages, while accurate, is costly and impractical.

*CONCLUSIONS*

The analysis of string behavior in the PM250 revealed that four “quarter-string” voltages can provide very good indication of the health of the string while requiring only four voltage measurements. Since this

technique isolates weak cells in the quarter string, the cell counterbalance problem of the earlier proposed “string imbalance” method is overcome.

## 6. References

G.J. Ball, G.C. Corey, and B.L. Norris, December 1994, *Government, Industry, and Utility Development and Evaluation of a Modular Utility Battery Energy Storage System*, presented at the winter meeting of the IEEE Power Engineering Society. New York, NY.

G.J. Ball, and B.L. Norris, March 1995, *AC Battery Test Report: Short-term System Characterization and Performance*, PG&E Research Report, Customer Systems Report 007.5-94.14. San Ramon, CA.

G. Corey, W. Nerbun, and D. Porter, August 1998, *Final Report on the Development of a 250-kW Modular, Factory-Assembled Battery Energy Storage System*, SAND97-1276. Sandia National Laboratories, Albuquerque, NM.

J.P. Holman, 1981, *Heat Transfer*. McGraw-Hill Book Company. New York, New York.

Institute of Electrical and Electronics Engineers, *IEEE Recommended Practices and Requirements for*

*Harmonic Control in Electric Power Systems*, IEEE Report No. 519-1992. 1992, New York, New York

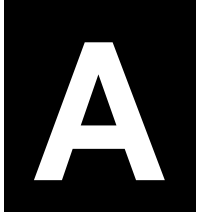
Institute of Electrical and Electronics Engineers, Power System Relaying Committee, Working Group C-5 of the Relaying Practices and Consumer Interface Subcommittee, 1994, *Summary of Static Power Converters of 500 kW or Less Serving as the Relay Interface Package for Non-Conventional Generators*. IEEE. 93THO 597-5 TWR (Reference No.). New York, New York

D. Linden, 1984, *Handbook of Batteries and Fuel Cells*. McGraw-Hill Publishing Company. New York, New York.

S. Virmani, G. Ball, and R. Zavadil, July 1994, *Dispersed System Impacts: Survey and Requirements Study*, Report No. TR-103337. Electric Power Research Institute. Palo Alto, CA.

This page intentionally left blank.

# Data Acquisition System



## Appendix A Data Acquisition System

The data acquisition system used during the PM250 prototype testing was incorporated by design into a PC-based supervisory control and data acquisition (SCADA) system. The design was intended to facilitate integration with Pacific Gas and Electric Company’s (PG&E’s) SCADA communications standards such that the system could easily be transported and installed in the field and controlled through one of PG&E’s dispatch centers.

The most common SCADA implementation at PG&E for both transmission and distribution control was on a VAX network using proprietary PG&E communications protocols. A low-cost alternative to the VAX package, however, was developed in-house by PG&E software developers and was gradually being introduced into the hydroelectric system and other niche locations.

*PC-SCADA for Windows* was the ideal platform to demonstrate control and data acquisition of the PM250 because it was low cost, provided for customization, and was fully compatible with the VAX standard.

The SCADA design incorporated two industry-standard RTUs for monitoring detailed module information (this equipment was provided by Electric Power Research Institute). Most container and gross module-level information was collected in a “master computer” in the container, which was programmed to communicate with the PG&E protocol. A detailed list of data points is provided in Appendix B.

Figure A-1 shows a block diagram of the SCADA/DAS configuration. Signals to the data acquisition system (DAS) system that indicate a hazard condition had parallel contacts to notify the site manager by pager. These signals include container smoke detection, excessive hydrogen detection, and system shutdown.

The sampling time of the DAS system for each channel was about 5 seconds; however, the number of averages was changed depending upon the requirements of each test. Typically, closely monitored tests include data averaged and stored each minute, while data between tests represented 15-minute intervals.

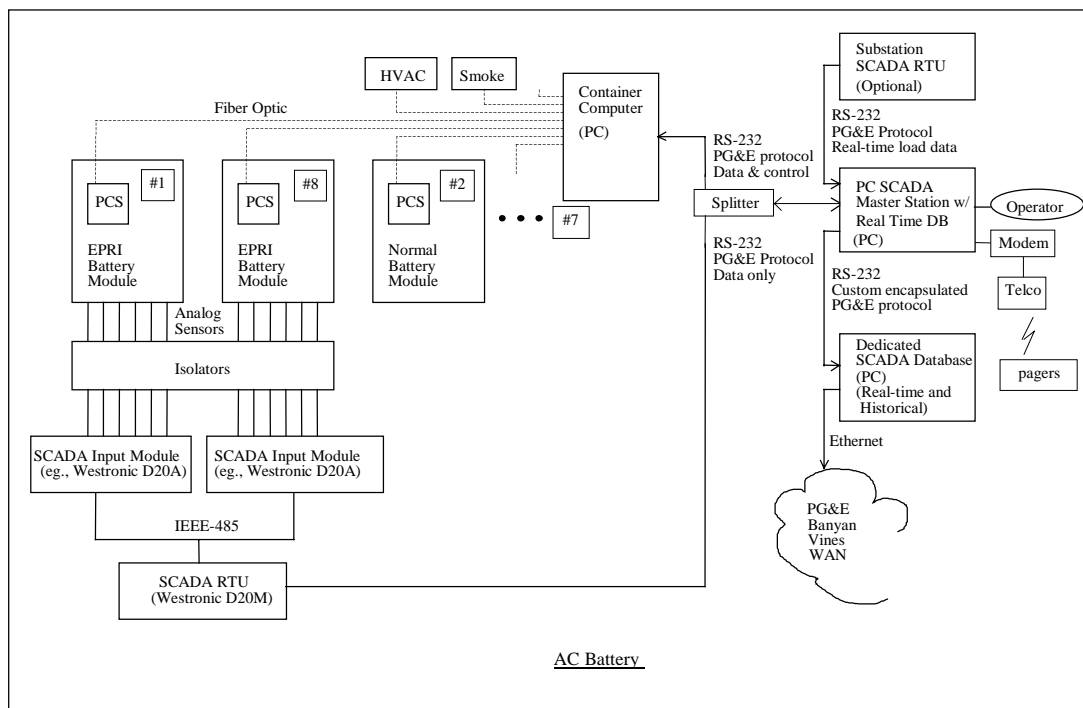


Figure A-1. SCADA and DAS system layout.

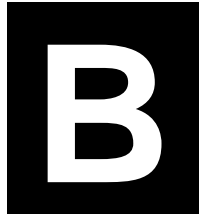
Table A-1 summarizes the system parameters and module-intensive parameters that were monitored or

calculated and maintained in the database.

**Table A-1. DAS Database Parameters**

DAS System Monitoring	Standard or EPRI data	Comments
<b>Measured Parameters</b>		
- DC string voltages (8)	S	1 per module
- sample battery voltages (18)	E	3 per the 6 non-intensive modules
- DC string currents (8)	S	1 per module
- ground currents (8)	S	1 per module; voltage measurement
- sample battery temperatures (8)	S	1 per module
- AC rms voltage (3)	E	container, 1 per phase
- AC rms current (3)	E	container, 1 per phase
- container kW (1)	E	3-phase measurement
- container kVAR (1)	E	3-phase measurement
- HVAC status (3)	S	on/off indication; cooler (2) and heater
- container temperature (1)	S	
- container hydrogen concentration (1)	S	
- container smoke detection (1)	S	
- control setpoints (19)	S	status of settings
<b>Calculated Parameters</b>		
- module kW <sub>dc</sub> (8)		
- module kW <sub>ac</sub> (8)		
- DC-AC efficiencies (9)		1 per module, and container aggregate
- module kVAR (8)		
- container power factor (1)		
- state of charge (SOC) (1)		Calculated from battery voltage
- energy available (1)		at present discharge rate
- discharge time remaining (1)		at present discharge rate
- cumulative energy in kWh (9)		module and aggregate
<b>Modules 1&amp;8 Measured Parameters</b>		
		(Intensively monitored)
- battery voltages (96)	E	2 modules, 48 batteries each
- string currents (2)	E	1 additional per module (4 total)
- battery temperatures (12)	E	6 per module
- inlet air temperatures (2)	E	1 per module
- outlet air temperatures (4)	E	3 per module
- PCS temperatures (6)	E	3 per module
- hydrogen concentration (2)	E	1 in manifold, 1 in Module 1
- system auxiliary power (1)	E	for HVAC effectiveness
- ambient temperature (1)	E	for container ambient conditions
- container temperatures (6)	E	additional for remaining 6 modules

# Points List



## Appendix B Points List

Table B-1 shows all of the parameters that were collected and archived through the SCADA system and associated data management tools. The *RTU* column indicates whether the point originated from the PM250 on-board master computer, one of the two module-level RTUs, or was calculated prior to

storage in the database. Note that some data were collected by independent PG&E instrumentation (the power transducer data and ambient temperature), and this was fed to the master computer using spare channels.

**Table B-1. SCADA Points List**

ID	RTU	Point Name	Units	Comments
1		Date/Time		Date and time of sample average.
2		FormatNum		
3		NumScans		
4	ACB_CONTAINER	VDC_STR1	V	String (module) voltage.
5	ACB_CONTAINER	VDC_STR2	V	String (module) voltage.
6	ACB_CONTAINER	VDC_STR3	V	String (module) voltage.
7	ACB_CONTAINER	VDC_STR4	V	String (module) voltage.
8	ACB_CONTAINER	VDC_STR5	V	String (module) voltage.
9	ACB_CONTAINER	VDC_STR6	V	String (module) voltage.
10	ACB_CONTAINER	VDC_STR7	V	String (module) voltage.
11	ACB_CONTAINER	VDC_STR8	V	String (module) voltage.
12	ACB_CONTAINER	IDC_STR1	A	String (module) current.
13	ACB_CONTAINER	IDC_STR2	A	String (module) current.
14	ACB_CONTAINER	IDC_STR3	A	String (module) current.
15	ACB_CONTAINER	IDC_STR4	A	String (module) current.
16	ACB_CONTAINER	IDC_STR5	A	String (module) current.
17	ACB_CONTAINER	IDC_STR6	A	String (module) current.
18	ACB_CONTAINER	IDC_STR7	A	String (module) current.
19	ACB_CONTAINER	IDC_STR8	A	String (module) current.
20	ACB_CONTAINER	VDC_GND1	V	Ground voltage.
21	ACB_CONTAINER	VDC_GND2	V	Ground voltage.
22	ACB_CONTAINER	VDC_GND3	V	Ground voltage.
23	ACB_CONTAINER	VDC_GND4	V	Ground voltage.
24	ACB_CONTAINER	VDC_GND5	V	Ground voltage.
25	ACB_CONTAINER	VDC_GND6	V	Ground voltage.
26	ACB_CONTAINER	VDC_GND7	V	Ground voltage.
27	ACB_CONTAINER	VDC_GND8	V	Ground voltage.
28	ACB_CONTAINER	TBAT_MOD1	DEG_C	Sample battery temperature in module.
29	ACB_CONTAINER	TBAT_MOD2	DEG_C	Sample battery temperature in module.

ID	RTU	Point Name	Units	Comments
30	ACB_CONTAINER	TBAT_MOD3	DEG_C	Sample battery temperature in module.
31	ACB_CONTAINER	TBAT_MOD4	DEG_C	Sample battery temperature in module.
32	ACB_CONTAINER	TBAT_MOD5	DEG_C	Sample battery temperature in module.
33	ACB_CONTAINER	TBAT_MOD6	DEG_C	Sample battery temperature in module.
34	ACB_CONTAINER	TBAT_MOD7	DEG_C	Sample battery temperature in module.
35	ACB_CONTAINER	TBAT_MOD8	DEG_C	Sample battery temperature in module.
36	ACB_CONTAINER	TPCS_MOD1	DEG_C	PCS heat sink temperature in module.
37	ACB_CONTAINER	TPCS_MOD2	DEG_C	PCS heat sink temperature in module.
38	ACB_CONTAINER	TPCS_MOD3	DEG_C	PCS heat sink temperature in module.
39	ACB_CONTAINER	TPCS_MOD4	DEG_C	PCS heat sink temperature in module.
40	ACB_CONTAINER	TPCS_MOD5	DEG_C	PCS heat sink temperature in module.
41	ACB_CONTAINER	TPCS_MOD6	DEG_C	PCS heat sink temperature in module.
42	ACB_CONTAINER	TPCS_MOD7	DEG_C	PCS heat sink temperature in module.
43	ACB_CONTAINER	TPCS_MOD8	DEG_C	PCS heat sink temperature in module.
44	ACB_CONTAINER	PAC_MOD_CTRL_PNT	KW	Container control point.
45	ACB_CONTAINER	Q_MOD_CTRL_PNT	KVAR	Container control point.
46	ACB_CONTAINER	PAC_CTRL_PNT	KW	Container control point.
47	ACB_CONTAINER	Q_CTRL_PNT	KVAR	Container control point.
48	ACB_CONTAINER	IAC_MOD_CTRL_PNT	A	Container control point.
49	ACB_CONTAINER	PAC	KW	Container meas power.
50	ACB_CONTAINER	Q	KVAR	Container meas reactive power
51	ACB_CONTAINER	IAC_PHA	A-RMS	Container meas AC current, A phase.
52	ACB_CONTAINER	IAC_PHB	A-RMS	Container meas AC current, B phase.
53	ACB_CONTAINER	IAC_PHC	A-RMS	Container meas AC current, C phase.
54	ACB_CONTAINER	VAC_PHA	V-RMS	Container AC voltage, AB phase.
55	ACB_CONTAINER	VAC_PHB	V-RMS	Container AC voltage, BC phase.
56	ACB_CONTAINER	VAC_PHC	V-RMS	Container AC voltage, CA phase.
57	ACB_CONTAINER	SOC	%	Container state of charge (SOC) (calc from battery voltage).
58	ACB_CONTAINER	AVAIL_KWH	%	Cont energy avail at discharge rate (calc).
59	ACB_CONTAINER	H2_CONC	%	Container hydrogen concentration (center).
60	ACB_CONTAINER	T_CONT	DEG_C	Container internal temperature.
61	ACB_CONTAINER	PAC_SET_PNT	KW	Container user requested power.
62	ACB_CONTAINER	Q_SET_PNT	KVAR	Container user requested reactive power.
63	ACB_CONTAINER	AVAIL_MIN	MIN	Time remaining at discharge rate (calc).
64	ACB_CONTAINER	SHUTDOWN	Digital	Status indicator - shutdown mode.
65	ACB_CONTAINER	STANDBY	Digital	Status indicator - standby mode.
66	ACB_CONTAINER	CHG_MODE	Digital	Status indicator - charge mode.
67	ACB_CONTAINER	DIS_MODE	Digital	Status indicator - discharge mode.
68	ACB_CONTAINER	AUTO_CHG_MODE	Digital	Status indicator - auto charge mode.
69	ACB_CONTAINER	END_OF_DISCHARGE	Digital	Status indicator - end of discharge.

ID	RTU	Point Name	Units	Comments
70	ACB_CONTAINER	TOP_OF_CHARGE	Digital	Status indicator - top of charge.
71	ACB_CONTAINER	CONS_VARS	Digital	Status indicator - consuming reactive power.
72	ACB_CONTAINER	PROD_VARS	Digital	Status indicator - producing reactive power.
73	ACB_CONTAINER	COOLER1_STS	Digital	Status indicator - coolers 1 & 2 on.
74	ACB_CONTAINER	COOLER2_STS	Digital	Status indicator - cooler 3&4 on.
75	ACB_CONTAINER	CONT_COLD	Digital	Status indicator - container under temp.
76	ACB_CONTAINER	SMK_ALRM	Digital	Status indicator - smoke in container.
77	ACB_CONTAINER	CONT_HOT	Digital	Status indicator - container over temp.
78	ACB_CONTAINER	H2_ALRM	Digital	Status indicator - excess hydrogen.
79	ACB_CONTAINER	E_STOP	Digital	Status indicator - emergency button pushed.
80	ACB_CONTAINER	ENABLE	Digital	Status indicator - enable switch on.
81	ACB_CONTAINER	CB_5227_STS	Digital	Status indicator - test facility breaker.
82	ACB_CONTAINER	H2_BLOWER	Digital	Status indicator - hydrogen blower on.
83	ACB_CONTAINER	DOOR_OPEN	Digital	Status indicator - container door open.
84	ACB_CONTAINER	COMM_ERR	Digital	Status indicator - communications error.
85	ACB_CONTAINER	CMD_INVALID	Digital	Status indicator - command invalid.
86	ACB_CONTAINER	FAULT_MOD1	Digital	Module Fault.
87	ACB_CONTAINER	FAULT_MOD2	Digital	Module Fault.
88	ACB_CONTAINER	FAULT_MOD3	Digital	Module Fault.
89	ACB_CONTAINER	FAULT_MOD4	Digital	Module Fault.
90	ACB_CONTAINER	FAULT_MOD5	Digital	Module Fault.
91	ACB_CONTAINER	FAULT_MOD6	Digital	Module Fault.
92	ACB_CONTAINER	FAULT_MOD7	Digital	Module Fault.
93	ACB_CONTAINER	FAULT_MOD8	Digital	Module Fault.
94	ACB_INTENSIVE_1	VDC_MOD1_BAT01	V	Single battery voltage.
95	ACB_INTENSIVE_1	VDC_MOD1_BAT02	V	Single battery voltage.
96	ACB_INTENSIVE_1	VDC_MOD1_BAT03	V	Single battery voltage.
97	ACB_INTENSIVE_1	VDC_MOD1_BAT04	V	Single battery voltage.
98	ACB_INTENSIVE_1	VDC_MOD1_BAT05	V	Single battery voltage.
99	ACB_INTENSIVE_1	VDC_MOD1_BAT06	V	Single battery voltage.
100	ACB_INTENSIVE_1	VDC_MOD1_BAT07	V	Single battery voltage.
101	ACB_INTENSIVE_1	VDC_MOD1_BAT08	V	Single battery voltage.
102	ACB_INTENSIVE_1	VDC_MOD1_BAT09	V	Single battery voltage.
103	ACB_INTENSIVE_1	VDC_MOD1_BAT10	V	Single battery voltage.
104	ACB_INTENSIVE_1	VDC_MOD1_BAT11	V	Single battery voltage. BAD: use est below.
105	ACB_INTENSIVE_1	VDC_MOD1_BAT12	V	Single battery voltage. BAD: use est below.
106	ACB_INTENSIVE_1	VDC_MOD1_BAT13	V	Single battery voltage.
107	ACB_INTENSIVE_1	VDC_MOD1_BAT14	V	Single battery voltage.
108	ACB_INTENSIVE_1	VDC_MOD1_BAT15	V	Single battery voltage.
109	ACB_INTENSIVE_1	VDC_MOD1_BAT16	V	Single battery voltage.

ID	RTU	Point Name	Units	Comments
110	ACB_INTENSIVE_1	VDC_MOD1_BAT17	V	Single battery voltage.
111	ACB_INTENSIVE_1	VDC_MOD1_BAT18	V	Single battery voltage.
112	ACB_INTENSIVE_1	VDC_MOD1_BAT19	V	Single battery voltage.
113	ACB_INTENSIVE_1	VDC_MOD1_BAT20	V	Single battery voltage.
114	ACB_INTENSIVE_1	VDC_MOD1_BAT21	V	Single battery voltage.
115	ACB_INTENSIVE_1	VDC_MOD1_BAT22	V	Single battery voltage.
116	ACB_INTENSIVE_1	VDC_MOD1_BAT23	V	Single battery voltage.
117	ACB_INTENSIVE_1	VDC_MOD1_BAT24	V	Single battery voltage.
118	ACB_INTENSIVE_1	VDC_MOD1_BAT25	V	Single battery voltage.
119	ACB_INTENSIVE_1	VDC_MOD1_BAT26	V	Single battery voltage.
120	ACB_INTENSIVE_1	VDC_MOD1_BAT27	V	Single battery voltage.
121	ACB_INTENSIVE_1	VDC_MOD1_BAT28	V	Single battery voltage.
122	ACB_INTENSIVE_1	VDC_MOD1_BAT29	V	Single battery voltage.
123	ACB_INTENSIVE_1	VDC_MOD1_BAT30	V	Single battery voltage.
124	ACB_INTENSIVE_1	VDC_MOD1_BAT31	V	Single battery voltage.
125	ACB_INTENSIVE_1	VDC_MOD1_BAT32	V	Single battery voltage.
126	ACB_INTENSIVE_1	VDC_MOD1_BAT33	V	Single battery voltage.
127	ACB_INTENSIVE_1	VDC_MOD1_BAT34	V	Single battery voltage.
128	ACB_INTENSIVE_1	VDC_MOD1_BAT35	V	Single battery voltage.
129	ACB_INTENSIVE_1	VDC_MOD1_BAT36	V	Single battery voltage.
130	ACB_INTENSIVE_1	VDC_MOD1_BAT37	V	Single battery voltage.
131	ACB_INTENSIVE_1	VDC_MOD1_BAT38	V	Single battery voltage.
132	ACB_INTENSIVE_1	VDC_MOD1_BAT39	V	Single battery voltage.
133	ACB_INTENSIVE_1	VDC_MOD1_BAT40	V	Single battery voltage.
134	ACB_INTENSIVE_1	VDC_MOD1_BAT41	V	Single battery voltage.
135	ACB_INTENSIVE_1	VDC_MOD1_BAT42	V	Single battery voltage.
136	ACB_INTENSIVE_1	VDC_MOD1_BAT43	V	Single battery voltage.
137	ACB_INTENSIVE_1	VDC_MOD1_BAT44	V	Single battery voltage.
138	ACB_INTENSIVE_1	VDC_MOD1_BAT45	V	Single battery voltage.
139	ACB_INTENSIVE_1	VDC_MOD1_BAT46	V	Single battery voltage.
140	ACB_INTENSIVE_1	VDC_MOD1_BAT47	V	Single battery voltage.
141	ACB_INTENSIVE_1	VDC_MOD1_BAT48	V	Single battery voltage.
142	ACB_INTENSIVE_1	T_MOD1_BAT01	DEG_C	Temperature of indicated battery.
143	ACB_INTENSIVE_1	T_MOD1_BAT03	DEG_C	Temperature of indicated battery.
144	ACB_INTENSIVE_1	T_MOD1_BAT16	DEG_C	Temperature of indicated battery. BAD
145	ACB_INTENSIVE_1	T_MOD1_BAT20	DEG_C	Temperature of indicated battery.
146	ACB_INTENSIVE_1	T_MOD1_BAT30	DEG_C	Temperature of indicated battery.
147	ACB_INTENSIVE_1	T_MOD1_BAT35	DEG_C	Temperature of indicated battery.
148	ACB_INTENSIVE_1	T_MOD1_BAT41	DEG_C	Temperature of indicated battery.
149	ACB_INTENSIVE_1	T_MOD1_BAT42	DEG_C	Temperature of indicated battery.

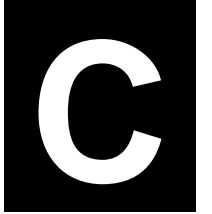
ID	RTU	Point Name	Units	Comments
150	ACB_INTENSIVE_1	T_IN_AIR_MOD1	DEG_C	Module inlet air temperature.
151	ACB_INTENSIVE_1	T_OUT_AIR1_MOD1	DEG_C	Module outlet air temperature.
152	ACB_INTENSIVE_1	T_OUT_AIR2_MOD1	DEG_C	Module outlet air temperature.
153	ACB_INTENSIVE_1	T_HT_SNK_MOD1	DEG_C	Module PCS heat sink temperature.
154	ACB_INTENSIVE_1	T_REACT_MOD1	DEG_C	Module reactor temperature.
155	ACB_INTENSIVE_1	IDC_POS_STR1	A	Module DC string current on positive section.
156	ACB_INTENSIVE_1	IDC_NEG_STR1	A	Module DC string current on negative section.
157	ACB_INTENSIVE_1	VDC_MOD8_BAT01	V	Single battery voltage.
158	ACB_INTENSIVE_1	VDC_MOD8_BAT02	V	Single battery voltage.
159	ACB_INTENSIVE_1	VDC_MOD8_BAT03	V	Single battery voltage.
160	ACB_INTENSIVE_1	VDC_MOD8_BAT04	V	Single battery voltage.
161	ACB_INTENSIVE_1	VDC_MOD8_BAT05	V	Single battery voltage.
162	ACB_INTENSIVE_1	VDC_MOD8_BAT06	V	Single battery voltage.
163	ACB_INTENSIVE_1	VDC_MOD8_BAT07	V	Single battery voltage.
164	ACB_INTENSIVE_1	VDC_MOD8_BAT08	V	Single battery voltage.
165	ACB_INTENSIVE_1	VDC_MOD8_BAT09	V	Single battery voltage.
166	ACB_INTENSIVE_1	VDC_MOD8_BAT10	V	Single battery voltage.
167	ACB_INTENSIVE_1	VDC_MOD8_BAT11	V	Single battery voltage.
168	ACB_INTENSIVE_1	VDC_MOD8_BAT12	V	Single battery voltage.
169	ACB_INTENSIVE_1	VDC_MOD8_BAT13	V	Single battery voltage.
170	ACB_INTENSIVE_1	VDC_MOD8_BAT14	V	Single battery voltage.
171	ACB_INTENSIVE_1	VDC_MOD8_BAT15	V	Single battery voltage.
172	ACB_INTENSIVE_1	VDC_MOD8_BAT16	V	Single battery voltage.
173	ACB_INTENSIVE_1	VDC_MOD8_BAT17	V	Single battery voltage.
174	ACB_INTENSIVE_1	VDC_MOD8_BAT18	V	Single battery voltage.
175	ACB_INTENSIVE_1	VDC_MOD8_BAT19	V	Single battery voltage. BAD: use est below.
176	ACB_INTENSIVE_1	VDC_MOD8_BAT20	V	Single battery voltage. BAD: use est below.
177	ACB_INTENSIVE_1	VDC_MOD8_BAT21	V	Single battery voltage.
178	ACB_INTENSIVE_1	VDC_MOD8_BAT22	V	Single battery voltage.
179	ACB_INTENSIVE_1	VDC_MOD8_BAT23	V	Single battery voltage.
180	ACB_INTENSIVE_1	VDC_MOD8_BAT24	V	Single battery voltage.
181	ACB_INTENSIVE_1	VDC_MOD8_BAT25	V	Single battery voltage.
182	ACB_INTENSIVE_1	VDC_MOD8_BAT26	V	Single battery voltage.
183	ACB_INTENSIVE_1	VDC_MOD8_BAT27	V	Single battery voltage.
184	ACB_INTENSIVE_1	VDC_MOD8_BAT28	V	Single battery voltage.
185	ACB_INTENSIVE_1	VDC_MOD8_BAT29	V	Single battery voltage.
186	ACB_INTENSIVE_1	VDC_MOD8_BAT30	V	Single battery voltage.
187	ACB_INTENSIVE_1	VDC_MOD8_BAT31	V	Single battery voltage.
188	ACB_INTENSIVE_1	VDC_MOD8_BAT32	V	Single battery voltage.
189	ACB_INTENSIVE_2	VDC_MOD8_BAT33	V	Single battery voltage.

ID	RTU	Point Name	Units	Comments
190	ACB_INTENSIVE_2	VDC_MOD8_BAT34	V	Single battery voltage.
191	ACB_INTENSIVE_2	VDC_MOD8_BAT35	V	Single battery voltage.
192	ACB_INTENSIVE_2	VDC_MOD8_BAT36	V	Single battery voltage.
193	ACB_INTENSIVE_2	VDC_MOD8_BAT37	V	Single battery voltage.
194	ACB_INTENSIVE_2	VDC_MOD8_BAT38	V	Single battery voltage.
195	ACB_INTENSIVE_2	VDC_MOD8_BAT39	V	Single battery voltage.
196	ACB_INTENSIVE_2	VDC_MOD8_BAT40	V	Single battery voltage.
197	ACB_INTENSIVE_2	VDC_MOD8_BAT41	V	Single battery voltage.
198	ACB_INTENSIVE_2	VDC_MOD8_BAT42	V	Single battery voltage.
199	ACB_INTENSIVE_2	VDC_MOD8_BAT43	V	Single battery voltage.
200	ACB_INTENSIVE_2	VDC_MOD8_BAT44	V	Single battery voltage.
201	ACB_INTENSIVE_2	VDC_MOD8_BAT45	V	Single battery voltage.
202	ACB_INTENSIVE_2	VDC_MOD8_BAT46	V	Single battery voltage.
203	ACB_INTENSIVE_2	VDC_MOD8_BAT47	V	Single battery voltage.
204	ACB_INTENSIVE_2	VDC_MOD8_BAT48	V	Single battery voltage.
205	ACB_INTENSIVE_2	T_MOD8_BAT01	DEG_C	Temperature on outside of indicated battery.
206	ACB_INTENSIVE_2	T_MOD8_BAT03	DEG_C	Temperature on outside of indicated battery.
207	ACB_INTENSIVE_2	T_MOD8_BAT16	DEG_C	Temperature on outside of indicated battery.
208	ACB_INTENSIVE_2	T_MOD8_BAT20	DEG_C	Temperature on outside of indicated battery.
209	ACB_INTENSIVE_2	T_MOD8_BAT30	DEG_C	Temperature on outside of indicated battery.
210	ACB_INTENSIVE_2	T_MOD8_BAT35	DEG_C	Temperature on outside of indicated battery.
211	ACB_INTENSIVE_2	T_MOD8_BAT41	DEG_C	Temperature on outside of indicated battery.
212	ACB_INTENSIVE_2	T_MOD8_BAT42	DEG_C	Temperature on outside of indicated battery.
213	ACB_INTENSIVE_2	T_IN_AIR_MOD8	DEG_C	Module inlet air temperature.
214	ACB_INTENSIVE_2	T_OUT_AIR1_MOD8	DEG_C	Module outlet air temperature.
215	ACB_INTENSIVE_2	T_OUT_AIR2_MOD8	DEG_C	Module outlet air temperature.
216	ACB_INTENSIVE_2	T_HT_SNK_MOD8	DEG_C	Module PCS heat sink temperature.
217	ACB_INTENSIVE_2	T_REACT_MOD8	DEG_C	Module reactor temperature.
218	ACB_INTENSIVE_2	IDC_POS_STR8	A	Module DC string current on positive section.
219	ACB_INTENSIVE_2	IDC_NEG_STR8	A	Module DC string current on negative section.
220	ACB_INTENSIVE_2	VDC_MOD2_BAT37	V	Sample battery voltage on indicated battery.
221	ACB_INTENSIVE_2	VDC_MOD2_BAT38	V	Sample battery voltage on indicated battery.
222	ACB_INTENSIVE_2	VDC_MOD2_BAT39	V	Sample battery voltage on indicated battery.
223	ACB_INTENSIVE_2	VDC_MOD3_BAT37	V	Sample battery voltage on indicated battery.
224	ACB_INTENSIVE_2	VDC_MOD3_BAT38	V	Sample battery voltage on indicated battery.
225	ACB_INTENSIVE_2	VDC_MOD3_BAT39	V	Sample battery voltage on indicated battery.
226	ACB_INTENSIVE_2	VDC_MOD4_BAT37	V	Sample battery voltage on indicated battery.
227	ACB_INTENSIVE_2	VDC_MOD4_BAT38	V	Sample battery voltage on indicated battery.
228	ACB_INTENSIVE_2	VDC_MOD4_BAT39	V	Sample battery voltage on indicated battery.
229	ACB_INTENSIVE_2	VDC_MOD5_BAT37	V	Sample battery voltage on indicated battery.

ID	RTU	Point Name	Units	Comments
230	ACB_INTENSIVE_2	VDC_MOD5_BAT38	V	Sample battery voltage on indicated battery.
231	ACB_INTENSIVE_2	VDC_MOD5_BAT39	V	Sample battery voltage on indicated battery.
232	ACB_INTENSIVE_2	VDC_MOD6_BAT37	V	Sample battery voltage on indicated battery.
233	ACB_INTENSIVE_2	VDC_MOD6_BAT38	V	Sample battery voltage on indicated battery.
234	ACB_INTENSIVE_2	VDC_MOD6_BAT39	V	Sample battery voltage on indicated battery.
235	ACB_INTENSIVE_2	VDC_MOD7_BAT37	V	Sample battery voltage on indicated battery.
236	ACB_INTENSIVE_2	VDC_MOD7_BAT38	V	Sample battery voltage on indicated battery.
237	ACB_INTENSIVE_2	VDC_MOD7_BAT39	V	Sample battery voltage on indicated battery.
238	ACB_INTENSIVE_2	T1_CONT_LO_NE_CRNR	DEG_C	Container temp lower NE corner.
239	ACB_INTENSIVE_2	T2_CONT_NW_AC_OUT	DEG_C	Container temp NW air cond inlet.
240	ACB_INTENSIVE_2	T3_CONT_NE_AC_OUT	DEG_C	Container temp NE air cond inlet.
241	ACB_INTENSIVE_2	T4_CONT_BOT_CNTR	DEG_C	Container temp bottom center.
242	ACB_INTENSIVE_2	T5_CONT_UP_SW_CRNR	DEG_C	Container temp high SW corner.
243	ACB_INTENSIVE_2	T6_CONT_SO_WALL	DEG_C	Container temp middle south wall.
244	ACB_INTENSIVE_2	T_AMB	DEG_C	Ambient temperature.
245	ACB_INTENSIVE_2	PAC_AUX	KW	Auxiliary power draw measured.
246	ACB_INTENSIVE_2	H2_CONC_MOD1	%	H2 conc in Module 1 (outside collector tubes).
247	ACB_INTENSIVE_2	H2_CONC_MANIF	%	H2 conc collected all Modules inside manifold.
248	CALCULATED	MOD1_BAT11C	V	Est bat voltage due to poor connection.
249	CALCULATED	MOD1_BAT12C	V	Est bat voltage due to poor connection.
250	CALCULATED	MOD8_BAT19C	V	Est bat voltage due to poor connection.
251	CALCULATED	MOD8_BAT20C	V	Est bat voltage due to poor connection.

This page intentionally left blank.

# List of Tests



## Appendix C List of Tests

Table C-1 shows an overview of the PM250 testing, commencing with the delivery of the system to San Ramon, California, and ending with the final short-term characterization tests. Longevity testing is not

shown, but was conducted through April 1994 by subjecting the system to a series of three-hour mock load-following cycles, and periodic standard baseline tests.

**Table C-1. PM250 Tests**

Date	Test Title	Comments
10/19/93	System Arrives	
10/23/93	Pre-parallel connection	
10/26/93	Pre-parallel connection 2	
10/26/93	Start-up and Internal Protection	
11/4/93	Baseline Test #2	The first baseline test performed at the Modular Generation Test Facility
11/5/93	Power Quality #1 and PF Control	BMI measurements; unable to accept signals 100-kHz spectrum analyzer single phase plots Nicolet storage RFI measurements from Julian Audio measurements from / (Peter Lee)
11/16/93	Battery Replacements	Not a test. Batteries 15 and 16 in Module 1 and battery #6 in Module 3 replaced.
11/17/93	40-minute block #1	190 kW Mod 2 imbalance SOC 32.9%
11/17/93	Harmonics Tests	BMI snapshots taken during 40-minute block discharge, 250-kW charge and autocharge.
11/18/93	1-hour block #1	167 kW Mod 6 imbalance SOC offset
11/19/93	2-hour block #1	92 kW Underproducing modules Communications problems Mods 6 & 2 imbalance 30.4% SOC
11/22/93	Module #4 responses	Few second delay of Module 4 during command change from standby to discharge. Confirmed via independent AC current clamp. (and audible)
11/24/93	Auxiliary power measurements	BMI snapshots taken on the input to aux transformer (CB9); Heater, different modes BMI on Module 8, to measure blower on/off etc... DAS measurements bogus

Date	Test Title	Comments
11/24/93	3-hour block #1	66 kW Utility power blip subsequent SCADA PC failure Module 6 imbalance
11/29/93	5-hour block #1	44 kW Incomplete communication failures smart-sub protection
1/28/94	Qualification test #1	
2/3/94	Qualification test #2	
2/3/94	Qualification test #3	Changed imbalance limits to +2 and -4 Vdc; Min string Vdc from 510 to 520 Vdc
2/14/94	1-hour block #2	155 kW Modules out on low voltage 520 Vdc 25% SOC
2/15/94	2-hour block #2	89 kW Vdc limit returned to 510 Vdc
2/16/94	3-hour block #2	65 kW
2/17/94	5-hour block #2	38 kW
2/21/94	40-minute block #2	205 kW
2/22/94	Islanding #1	Battery 100 kW, load bank 20-200 kW 108 kW matching tests
2/23/94	Islanding #2	Matching 100 kW, varied VARs $\pm$ 50 kVAR 208 kW matching 0 kVAR producing vs. consuming Reclose tests
2/23/94	Speed and Stability	Response from SCADA and PCS to mode changes DC injection problems
2/24/94	2-hour load follow #1 (equivalent)	Two humped equivalent to a single 2-hour sine
2/24/94	Module harmonics test	Harmonics from 8-1 operating modules planned Unable to run less than 4 at a time Sensitive to particular module on
2/25/94	3-hour load follow	96 kW peak
2/28/94	2-hour load follow #2	134.3 kW peak
3/1/94	4-hour load follow	75.5 kW peak
3/2/94	5-hour load follow #1	62.1 kW peak
3/7/94	8-hour load follow #1	Cancelled midstream for bad SOC calculations
3/7/94	5-hour load follow #2	62.1 kW Ran with corrected SOC calculation immediately followed the failed 8-hour attempt
3/8/94	Opportunity charge #1	2-hour load follow discharge to 25% 2-hour sine charge 2-hour load follow Shutdown early on SOC
3/14/94	8-hour load follow #2	38 kW peak

---

---

Date	Test Title	Comments
3/15/94	Opportunity Charge #2	Different charge/discharge thresholds 2 hour load follow? Deep charge load follow/problems accepting >265 kW 1.5 hour discharge
3/15/94	Container power tests	Discrepancies between requested, commanded, DAS and PQnode measurements recorded.
3/21/94	250-kW block discharge	Approx. 26-minute test to 25% SOC Modules out on low Vdc (voltage).

---

---

This page intentionally left blank.

## Distribution

Bob Weaver  
777 Wildwood Lane  
Palo Alto, CA 94303

Per Danfors  
ABB Power T&D Co., Inc.  
16250 West Glendale Drive  
New Berlin, WI 53151

Jim Balthazar  
Active Power  
11525 Stonehollow Dr.  
Suite 255  
Austin, TX 78758

Robert Wills  
Advanced Energy Systems  
Riverview Mill  
P.O. Box 262  
Wilton, NH 03086

Percy Frisbey  
Alaska State Div. of Energy  
333 West Fourth Ave.  
Suite 220  
Anchorage, AK 99501-2341

Michael L. Gravely  
American Superconductor Corp.  
8371 Bunchberry Court  
Citrus Heights, CA 95610

Meera Kohler  
Anchorage Municipal Light & Pwr  
1200 East 1st Avenue  
Anchorage, AK 99501

Tim Ball  
Applied Power Corporation  
Solar Engineering  
1210 Homann Drive SE  
Lacey, WA 98503

Ralph M. Nigro  
Applied Energy Group, Inc.  
46 Winding Hill Drive  
Hockessin, DE 19707

Christian St-Pierre  
ARGO-TECH Productions, Inc.  
Subsidiary of Hydro-Quebec  
1580 de Coulomb  
Boucherville, QC J4B 7Z7  
CANADA

Gary Henriksen  
Argonne National Laboratories  
9700 South Cass Avenue  
CTD, Bldg. 205  
Argonne, IL 60439

Herb Hayden  
Arizona Public Service  
400 North Fifth Street  
P.O. Box 53999, MS8931  
Phoenix, AZ 85072-3999

Ray Hobbs  
Arizona Public Service  
400 North Fifth Street  
P.O. Box 5399, MS8931  
Phoenix, AZ 85072-3999

Robert Hammond  
Arizona State University East  
6001 S. Power Rd.  
Bldg. 539  
Mesa, AZ 85206

Edward C. Kern  
Ascension Technology, Inc.  
P.O. Box 6314  
Lincoln, MA 01773-6314

Glenn Campbell  
Babcock & Wilcox  
P.O. Box 785  
Lynchburg, VA 24505

Richard L. Hockney  
Beacon Power Corp.  
6 Gill St.  
Woburn Industrial Park  
Woburn, MA 01801-1721

Michael L. Bergey  
Bergey Windpower  
2001 Priestley Avenue  
Norman, OK 73069

Klaus Kramer  
Berliner Kraft und Licht (BEWAG)  
Stauffenbergstrasse 26  
1000 Berlin 30  
GERMANY

Massoud Assefpour  
BHP Research & Tech Dev.  
600 Bourke Street  
Melbourne Victoria, 3000  
AUSTRALIA

Samuel B. Wright  
Boeing  
Inform., Space & Defense Sys.  
P.O. Box 3999 MS 82-97  
Seattle, WA 98124-2499

Gerald W. Braun  
BP Solarex  
630 Solarex Court  
Frederick, MD 21703

Dr. Sudhan S. Misra  
C&D Charter Pwr. Systems, Inc.  
Washington & Cherry Sts.  
Conshohocken, PA 19428

Dr. Les Holden  
C&D Charter Pwr. Systems, Inc.  
Washington & Cherry Sts.  
Conshohocken, PA 19428

Larry S. Meisner  
C&D Powercom  
1400 Union Meeting Road  
P.O. Box 3053  
Blue Bell, PA 19422-0858

Jon Edwards  
California Energy Commission  
1516 Ninth Street, MS-46  
Sacramento, CA 95814

Pramod P. Kulkarni  
California Energy Commission  
Research & Dev. Office  
1516 9th Street, MS43  
Sacramento, CA 95814-5512

Tom Lovas  
Chugach Elec. Association, Inc.  
P.O. Box 196300  
Anchorage, AK 99519-6300

John Cooley  
Chugach Elec. Association, Inc.  
P.O. Box 196300  
Anchorage, AK 99519-6300

R. B. Sloan  
Crescent EMC  
P.O. Box 1831  
Statesville, NC 28687

J. Michael Hinga  
Delphi Energy & Engine  
Management Systems  
P.O. Box 502650  
Indianapolis, IN 46250

Bob Rider  
Delphi Energy & Engine  
Management Systems  
P.O. Box 502650  
Indianapolis, IN 46250

Albert R. Landgrebe  
Department of Energy - Retired  
B14 Suffex Lane  
Millsboro, DE 19966

Joseph J. Iannucci  
Distributed Utility Associates  
1062 Concannon Blvd.  
Livermore, CA 94550

Alan Collinson  
EA Technology Limited  
Chester CH1 6ES  
Capenhurst, England  
UNITD KINGDOM

Jim DeGruson  
Eagle-Picher Industries. Inc.  
C & Porter Street  
Joplin, MO 64802

M. Stanton  
East Penn Manufact. Co., Inc.  
Deka Road  
Lyon Station, PA 19536

Phillip C. Symons  
Electrochemical Engineering  
Consultants, Inc.  
1295 Kelly Park Circle  
Morgan Hill, CA 95037

Dave Feder  
Electrochemical Energy  
Storage Systems, Inc.  
35 Ridgedale Avenue  
Madison, NJ 07940

Michael Dodge  
Electrosource  
P.O. Box 7115  
Loveland, CO 80537

Harald Haegermark  
Elforsk-Swedish Elec Utilities R&D Co  
Elforsk AB  
Stockholm, S-101 53  
Sweden

Eric Rudd  
Eltech Research Corporation  
625 East Street  
Fairport Harbor, OH 44077

Jennifer Schilling  
Energetics  
501 School Street SW  
Suite 500  
Washington, DC 20024

Phil DiPietro  
Energetics  
501 School Street SW  
Suite 500  
Washington, DC 20024

Paula A. Taylor  
Energetics  
7164 Gateway Drive  
Columbia, MD 21046

Mindi J. Farber-DeAnda  
Energetics  
501 School Street SW  
Suite 500  
Washington, DC 20024

Howard Lowitt  
Energetics  
7164 Gateway Drive  
Columbia, MD 21046

Rich Scheer  
Energetics  
501 School Street SW  
Suite 500  
Washington, DC 20024

Laura Johnson  
Energetics, Inc.  
7164 Gateway Drive  
Columbia, MD 21046

Greg J. Ball  
Energy & Env. Economics, Inc.  
353 Sacramento Street  
Suite 1540  
San Francisco, CA 94111

Amber Gray-Fenner  
Energy Communications Consulting  
7204 Marigot Rd. NW  
Albuquerque, NM 87120

Al Pivec  
Energy Systems Consulting  
41 Springbrook Road  
Livingston, NJ 07039

Dale Butler  
EnerTec Pty. Ltd.  
349 Coronation Drive  
PO Box 1139, Milton BC Old 4044  
Auchenflower, Queensland, 4066  
AUSTRALIA

David H. DaCosta  
Ergenics, Inc.  
247 Margaret King Avenue  
Ringwood, NJ 07456

Erik Hennig  
EUS GmbH  
MunscheidstraBe 14  
Gelsenkirchen, 45886  
Germany

John Breckenridge  
Exide Electronics  
8609 Six Forks Road  
Raleigh, NC 27615

James P. Dunlop  
Florida Solar Energy Center  
1679 Clearlake Road  
Cocoa, FL 32922-5703

Steven J. Durand  
Florida Solar Energy Center  
1679 Clearlake Road  
Cocoa, FL 32922-5703

Steven Kraft  
Frost & Sullivan  
2525 Charleston Road  
Mountain View, CA 94043

Bob Zrebiec  
GE Industrial & Pwr. Services  
640 Freedom Business Center  
King of Prussia, PA 19046

Nick Miller  
General Electric Company  
1 River Road  
Building 2, Room 605  
Schenectady, NY 12345

Declan Daly  
General Electric Drive Systems  
1501 Roanoke Blvd.  
Salem, VA 24153

Gerry Woolf  
Gerry Woolf Associates  
17 Westmeston Avenue  
Rottingdean, East Sussex, BN2 8AL  
UNITED KINGDOM

Anthony B. LaConti  
Giner, Inc.  
14 Spring Street  
Waltham, MA 02451-4497

George Hunt  
GNB Tech. Ind. Battery Co.  
Woodlake Corporate Park  
829 Parkview Blvd.  
Lombard, IL 60148-3249

Joe Szymborski  
GNB Tech. Ind. Battery Co.  
Woodlake Corporate Park  
829 Parkview Blvd.  
Lombard, IL 60148-3249

Sanjay Deshpande'  
GNB Technologies  
Woodlake Corporate Park  
829 Parkview Blvd.  
Lombard, IL 60148-3249

J. Boehm  
GNB Tech. Ind. Battery Co.  
Woodlake Corporate Park  
829 Parkview Blvd.  
Lombard, IL 60148-3249

Steven Haagensen  
Golden Valley Elec. Assoc., Inc.  
758 Illinois Street  
P.O. Box 71249  
Fairbanks, AK 99701

Ben Norris  
Gridwise Engineering Company  
121 Starlight Place  
Danville, CA 94526

Clyde Nagata  
Hawaii Electric Light Co.  
P.O. Box 1027  
Hilo, HI 96720

Carl Parker  
ILZRO  
2525 Meridian Parkway  
P.O. Box 12036  
Research Triangle Park, NC 27709

Patrick Moseley  
ILZRO  
2525 Meridian Parkway  
P.O. Box 12036  
Research Triangle Park, NC 27709

Jerome F. Cole  
ILZRO  
2525 Meridian Parkway  
PO Box 12036  
Research Triangle Park, NC 27709

Ken Belfer  
Innovative Power Sources  
1419 Via Jon Jose Road  
Alamo, CA 94507

A. Kamal Kalafala  
Intermagnetics General Corp.  
450 Old Niskayuna Road  
P.O. Box 461  
Latham, NY 12110-0461

John Neal  
International Business & Tech.  
Services, Inc.  
9220 Tayloes Neck Road  
Nanjemoy, MD 20662

Gerard H. C. M. Thijssen  
KEMA T&D Power  
Utrechtseweg 310  
P.O. Box 9035  
ET, Ernhem, 6800  
The Netherlands

Elton Cairns  
Lawrence Berkeley Nat'l Lab  
University of California  
One Cyclotron Road  
Berkeley, CA 94720

Frank McLarnon  
Lawrence Berkeley National Lab  
University of California  
One Cyclotron Road  
Berkeley, CA 94720

Kim Kinoshita  
Lawrence Berkeley Nat'l Lab  
University of California  
One Cyclotron Road  
Berkeley, CA 94720

J. Ray Smith  
Lawrence Livermore Nat'l Lab  
University of California  
P.O. Box 808, L-641  
Livermore, CA 94551

Susan Marie Schoenung  
Longitude 122 West, Inc.  
1010 Doyle Street  
Suite 10  
Menlo Park, CA 94025

Joseph Morabito  
Lucent Technologies, Inc.  
600 Mountain View Ave.  
P.O. Box 636  
Murray Hill, NJ 07974-0636

Cecilia Y. Mak  
Lucent Technologies  
3000 Skyline Drive  
Room 855  
Mesquite, TX 75149-1802

Stephen R. Connors  
Massachusetts Inst of Tech  
The Energy Laboratory  
Rm E40-465  
Cambridge, MA 02139-4307

Dutch Achenbach  
Metlakatla Power & Light  
P.O. Box 359  
3.5 Mile Airport Road  
Metlakatla, AK 99926

Dr. Christine E. Platt  
Nat'l Institute of Standards & Tech.  
Room A225 Administration Bldg.  
Gaithersburg, MD 20899

Byron Stafford  
Nat'l Renewable Energy Lab  
1617 Cole Boulevard  
Golden, CO 80401-3393

Holly Thomas  
Nat'l Renewable Energy Lab  
1617 Cole Boulevard  
Golden, CO 80401-3393

Richard DeBlasio  
Nat'l Renewable Energy Lab  
1617 Cole Boulevard  
Golden, CO 80401-3393

Jim Green  
Nat'l Renewable Energy Lab  
1617 Cole Boulevard  
Golden, CO 80401-3393

Larry Flowers  
Nat'l Renewable Energy Lab  
1617 Cole Boulevard  
Golden, CO 80401-3393

Susan Hock  
Nat'l Renewable Energy Lab  
1617 Cole Boulevard  
Golden, CO 80401-3393

Anthony Price  
National Power PLC  
Harwell Int'l Business Ctr.  
Harwell, Didcot, OX11 0QA  
London

Steven P. Lindenberg  
National Rural Elec Cooperative Assoc.  
4301 Wilson Blvd.  
SSER9-207  
Arlington, VA 22203-1860

Bill Brooks  
NC Solar Center  
Corner of Gorman & Western  
Box 7401 NCSU  
Raleigh, NC 27695-740

Andrew L. Rosenthal  
New Mexico State University  
Southwest Tech. Dev. Institute  
Box 30001/Dept. 3SOL  
Las Cruces, NM 88003-8001

Denise Zurn  
Northern States Power Co.  
414 Nicollet Mall  
Minneapolis, MN 55401

John Stoval  
Oak Ridge National Laboratory  
P.O. Box 2008  
Bldg. 3147, MS-6070  
Oak Ridge, TN 37831-6070

Robert Hawsey  
Oak Ridge National Laboratory  
P.O. Box 2008  
Bldg. 3025, MS-6040  
Oak Ridge, TN 37831-6040

James VanCoevering  
Oak Ridge National Laboratory  
P.O. Box 2008  
Bldg. 3147, MS-6070  
Oak Ridge, TN 37831-6070

Brendan Kirby  
Oak Ridge National Laboratory  
P.O. Box 2008  
Bldg. 3147, MS-6070  
Oak Ridge, TN 37831-6070

Hans Meyer  
Omnion Pwr. Engineering Corp.  
2010 Energy Drive  
P.O. Box 879  
East Troy, WI 53120

Douglas R. Danley  
Orion Energy Corporation  
10087 Tyler Place #5  
Ijamsville, MD 21754

Thomas H. Schucan  
Paul Scherrer Institut  
CH - 5232 Villigen PSI  
Switzerland

Brad Johnson  
PEPCO  
1900 Pennsylvania NW  
Washington, DC 20068

Stan Sostrom  
POWER Engineers, Inc.  
P.O. Box 777  
3870 US Hwy 16  
Newcastle, WY 82701

P. Prabhakara  
Power Technologies, Inc.  
1482 Erie Blvd.  
P.O. Box 1058  
Schenectady, NY 12301

Henry W. Zaininger  
Power Technologies, Inc.  
775 Sunrise Avenue  
Suite 210  
Roseville, CA 95661

Rick Winter  
Powercell Corporation  
101 Main Street  
Suite 9  
Cambridge, MA 02142-1519

Reznor I. Orr  
Powercell Corporation  
101 Main Street  
Suite 9  
Cambridge, MA 02142-1519

Jerry Neal  
Public Service Co. of New Mexico  
Alvarado Square MS-BA52  
Albuquerque, NM 87158

Roger Flynn  
Public Service Co. of New Mexico  
Alvarado Square MS-2838  
Albuquerque, NM 87158

Wenceslao Torres  
Puerto Rico Elec. Pwr. Authority  
G.P.O. Box 4267  
San Juan, PR 00936-426

Norman Lindsay  
Queensland Department of  
Mines and Energy  
G.P.O. Box 194  
Brisbane, 4001  
QLD. AUSTRALIA

Michael C. Saft  
SAFT Research & Dev. Ctr.  
107 Beaver Court  
Cockeysville, MD 21030

G. E. "Ernie" Palomino  
Salt River Project  
P.O. Box 52025  
MS PAB 357  
Phoenix, AZ 85072-2025

H. Lundstrom  
Salt River Project  
P.O. Box 52025  
MS PAB 357  
Phoenix, AZ 85072-2025

Robert Reeves  
Sentech, Inc.  
9 Eaton Road  
Troy, NY 12180

Kurt Klunder  
Sentech, Inc.  
4733 Bethesda Avenue  
Suite 608  
Bethesda, MD 20814

Rajat K. Sen  
Sentech, Inc.  
4733 Bethesda Avenue  
Suite 608  
Bethesda, MD 20814

Nicole Miller  
Sentech, Inc.  
4733 Bethesda Avenue  
Suite 608  
Bethesda, MD 20814

Clay Aldrich  
Siemens Solar  
4650 Adohr Lane  
P.O. Box 6032  
Camarillo, CA 93011

Deepak Divan  
Soft Switching Technologies  
2224 Evergreen Road  
Suite 6  
Middleton, WI 53562

Scott Sklar  
Solar Energy Ind. Assoc. (SEIA)  
122 C Street NW  
4th Floor  
Washington, DC 20001-2104

Naum Pinsky  
Southern California Edison  
2244 Walnut Grove Ave.  
P.O. Box 800, Room 418  
Rosemead, CA 91770

Bruce R. Rauhe, Jr.  
Southern Company Services, Inc.  
600 North 18th Street  
P.O. Box 2625  
Birmingham, AL 35202-2625

Richard N. Schweinberg  
Southern California Edison  
6070 N. Irwindale Avenue  
Suite I  
Irwindale, CA 91702

George Zink  
Stored Energy Engineering  
7601 E. 88th Place  
Indianapolis, IN 46256

Bob Bish  
Stored Energy Engineering  
7601 E. 88th Place  
Indianapolis, IN 46256

Jon Hurwitch  
Switch Technologies  
4733 Bethesda Avenue  
Suite 608  
Bethesda, MD 20814

Thomas J. Jenkin  
The Brattle Group  
44 Brattle Street  
Cambridge, MA 02138-3736

Haukur Asgeirsson  
The Detroit Edison Company  
2000 2nd Ave.  
435 SB  
Detroit, MI 48226-1279

Charles E. Bakis  
The Pennsylvania State University  
227 Hammond Building  
University Park, PA 16802

Michael Orians  
The Solar Connection  
P.O. Box 1138  
Morro Bay, CA 93443

Tom Anyos  
The Technology Group, Inc.  
63 Linden Avenue  
Atherton, CA 94027-2161

Bill Roppenecker  
Trace Engineering Division  
5916 195th Northeast  
Arlington, WA 98223

Bill Erdman  
Trace Technologies  
6952 Preston Avenue  
Livermore, CA 94550

Michael Behnke  
Trace Technologies  
6952 Preston Ave.  
P.O. Box 5049  
Livermore, CA 94550

Donald A. Bender  
Trinity Flywheel Power  
6724D Preston Avenue  
Livermore, CA 94550

Jim Drizos  
Trojan Battery Company  
12380 Clark Street  
Santa Fe Springs, CA 90670

James Fanguie  
TU Electric  
R&D Programs  
P.O. Box 970  
Fort Worth, TX 76101

Paul C. Klimas  
U.S. Agency for Intn'l Development  
Center for Environment  
Washington, DC 20523-3800

Jim Daley  
U.S. Department of Energy  
1000 Independence Ave. SW  
EE-12 FORSTL  
Washington, DC 20585

Dan T. Ton  
U.S. Department of Energy  
1000 Independence Ave. SW  
EE-11 FORSTL  
Washington, DC 20585

James E. Rannels  
U.S. Department of Energy  
1000 Independence Ave. SW  
EE-11 FORSTL  
Washington, DC 20585-0121

Gary A. Buckingham  
U.S. Department of Energy  
Albuquerque Operations Office  
P.O. Box 5400  
Albuquerque, NM 87185

Alex O. Bulawka  
U.S. Department of Energy  
1000 Independence Ave. SW  
EE-11 FORSTL  
Washington, DC 20585

J. A. Mazer  
U.S. Department of Energy  
1000 Independence Ave. SW  
EE-11 FORSTL  
Washington, DC 20585

Richard J. King  
U.S. Department of Energy  
1000 Independence Ave. SW  
EE-11 FORSTL, 5H-095  
Washington, DC 20585

Russ Eaton  
U.S. Department of Energy  
Golden Field Office  
1617 Cole Blvd., Bldg. 17  
Golden, CO 80401

Kenneth L. Heitner  
U.S. Department of Energy  
1000 Independence Ave. SW  
EE-32 FORSTL  
Washington, DC 20585

Neal Rossmeyssl  
U.S. Department of Energy  
1000 Independence Ave. SW  
EE-13 FORSTL  
Washington, DC 20585

Allan Jelacic  
U.S. Department of Energy  
1000 Independence Ave. SW  
EE-12 FORSTL  
Washington, DC 20585

Philip N. Overholt  
U.S. Department of Energy  
1000 Independence Ave. SW  
EE-11 FORSTL  
Washington, DC 20585-0121

Jack Cadogan  
U.S. Department of Energy  
1000 Independence Ave. SW  
EE-11 FORSTL  
Washington, DC 20585

Joe Galdo  
U.S. Department of Energy  
1000 Independence Ave. SW  
EE-10 FORSTL  
Washington, DC 20585

Dr. Gerald P. Ceasar  
U.S. Department of Commerce  
NIST/ATP  
Bldg 101, Room 623  
Gaithersburg, MD 20899

Dr. Imre Gyuk  
U.S. Department of Energy  
1000 Independence Ave. SW  
EE-14 FORSTL  
Washington, DC 20585

Bob Brewer  
U.S. Department of Energy  
1000 Independence Ave. SW  
EE-10 FORSTL  
Washington, DC 20585

Steve Bitterly  
U.S. Flywheel Systems  
1125-A Business Center Circle  
Newbury Park, CA 91320

Wayne Taylor  
U.S. Navy  
Code 83B000D, NAWS  
China Lake, CA 93555

Edward Beardsworth  
UFTO  
951 Lincoln Avenue  
Palo Alto, CA 94301-3041

Tien Q. Duong  
United States Department of Energy  
1000 Independence Ave. SW  
EE-32 FORSTL, Rm. 5G-030  
Washington, DC 20585

John Herbst  
University of Texas at Austin  
J.J. Pickel Research Campus  
Mail Code R7000  
Austin, TX 78712

Max Anderson  
University of Missouri - Rolla  
112 Electrical Eng. Bldg.  
Rolla, MO 65401-0249

G. Alan Palin  
Urenco (Capenhurst) Ltd.  
Capenhurst, Chester, CH1 6ER  
UNITED KINGDOM

Steve Hester  
Utility Photo Voltaic Group  
1800 M Street NW  
Washington, DC 20036-5802

Mike Stern  
Utility Power Group  
9410-G DeSoto Avenue  
Chatsworth, CA 91311-4947

Alex Q. Huang  
Virginia Polytechnic Instit. & State Uni  
Virginia Power Electronics Center  
672 Whittemore Hall  
Blacksburg, VA 24061

Howard Saunders  
Westinghouse STC  
1310 Beulah Road  
Pittsburgh, PA 15235

Frank Tarantino  
Yuasa, Inc.  
2366 Bernville Road  
P.O. Box 14145  
Reading, PA 19612-4145

Nicholas J. Magnani  
Yuasa, Inc.  
2366 Bernville Road  
P.O. Box 14145  
Reading, PA 19612-4145

Gene Cook  
Yuasa, Inc.  
2366 Bernville Road  
P.O. Box 14145  
Reading, PA 19612-4145

Robert J. Parry  
ZBB Technologies  
11607 West Dearbourn Ave.  
Wauwatosa, WI 53226-3961

MS-0619, Review & Approval For DOE/OSTI (00111) (1)  
MS-0212, Andrew Phillips (10230)  
MS-0340, Jeff W. Braithwaite (1832)  
MS-0457, Gary N. Beeler (2000)  
MS-0537, Stan Atcitty (2314)  
MS-0953, William E. Alzheimer (2500)  
MS-0953, Thomas J. Cutchen (2500)  
MS-0613, Daniel H. Doughty (2521)  
MS-0613, Rudy G. Jungst (2521)  
MS-0613, Terry Unkelhaeuser (2521)  
MS-0614, Dennis E. Mitchell (2522)  
MS-0614, Robert W. Bickes (2523)  
MS-0613, John D. Boyes (2525)  
MS-0613, Paul C. Butler (2525) (10)  
MS-0613, Nancy H. Clark (2525)  
MS-0613, Garth P. Corey (2525)  
MS-0613, Terry Crow (2525)  
MS-0613, Imelda Francis (2525)  
MS-0613, Gus P. Rodriguez (2525)  
MS-0899, Technical Library (4916) (2)  
MS-0741, Sam Varnado (6200)  
MS-0704, Abbas A. Akhil (6201)  
MS-0708, Henry M. Dodd (6214)  
MS-0753, Russell H. Bonn (6218)  
MS-0753, Ward I. Bower (6218)  
MS-0753, Christopher Cameron (6218)  
MS-0753, Tom Hund (6218)  
MS-0753, John W. Stevens (6218)  
MS-0455, Marjorie L. Tatro (6231)  
MS-9403, Jim Wang (8713)  
MS-9018, Central Technical Files (8940-2)  
MS-1193, Dean C. Rovang (9531)